AD-A089 215 WISCONSIN UNIV-MADISON DEPT OF CHEMISTRY F/G 7/4
LUMINESCENT PROPERTIES OF SEMICONDUCTOR PHOTOELECTRODES.(U)
AUG 80 A B ELLIS, B R KARAS N00014-78-C-0633
UNCLASSIFIED TR-1 NL

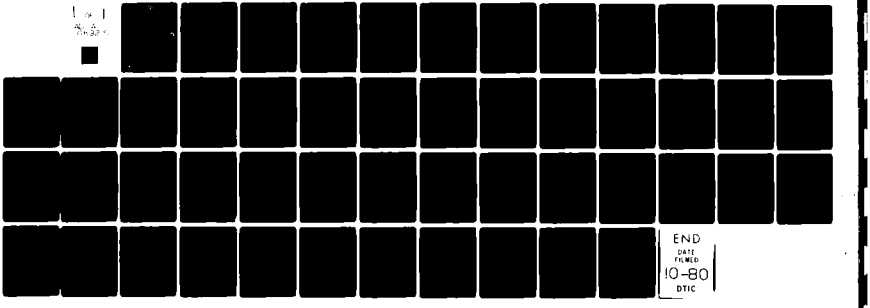

END
DATE FILMED
10-80
DTIC

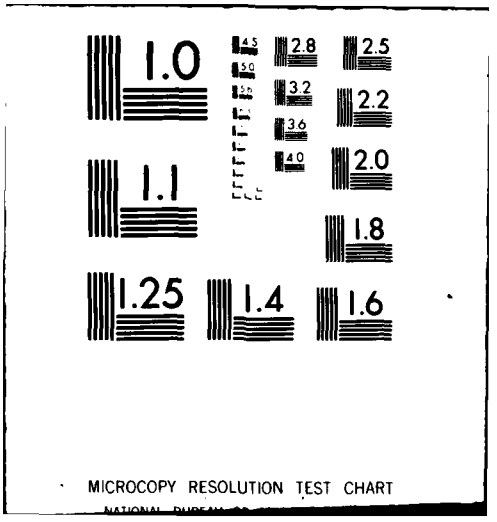
1.0
1.1
1.25
1.4
1.6
1.8
2.0
2.2
2.5
2.8
3.2
3.6
4.0
4.5
5.0
MICROCOPY RESOLUTION TEST CHART

LEVEL II

12

OFFICE OF NAVAL RESEARCH

Contract No. N00014-78-C-0633

Task No. NR 051-690

TECHNICAL REPORT NO. 1

Luminescent Properties of Semiconductor Photoelectrodes

by

Arthur B. Ellis* and Bradley R. Karas

Prepared for Publication

in

Advances in Chemistry Series

Department of Chemistry
University of Wisconsin
Madison, Wisconsin 53706

August 12, 1980

*To whom all correspondence should be addressed.

UNCLASSIFIED

SECURITY CLASSIFICATION OF THIS PAGE (When Data Entered)

REPORT DOCUMENTATION PAGE	READ INSTRUCTIONS BEFORE COMPLETING FORM
(9) 1. REPORT NUMBER: Technical Report No. 1 / 2. GOVT ACCESSION NO.: AD-A089 215	3. RECIPIENT'S CATALOG NUMBER
(6) 4. TITLE (and Subtitle): Luminescent Properties of Semiconductor Photoelectrodes.	(11) 5. TYPE OF REPORT & PERIOD COVERED: 12 Aug 80
	6. PERFORMING ORG. REPORT NUMBER
(10) 7. AUTHOR(s): Arthur B. Ellis and Bradley R. Karas	(15) 8. CONTRACT OR GRANT NUMBER(s): N00014-78-C-0633
9. PERFORMING ORGANIZATION NAME AND ADDRESS: Department of Chemistry, University of Wisconsin, Madison, Wisconsin 53706 (14) TR-1	10. PROGRAM ELEMENT, PROJECT, TASK AREA & WORK UNIT NUMBERS: NR 051-690 (12) 51
11. CONTROLLING OFFICE NAME AND ADDRESS: Office of Naval Research/Chemistry Program, Arlington, VA 22217	12. REPORT DATE: August 12, 1980
	13. NUMBER OF PAGES: 29 42
14. MONITORING AGENCY NAME & ADDRESS (if different from Controlling Office)	15. SECURITY CLASS. (of this report): Unclassified
	15a. DECLASSIFICATION/DOWNGRADING SCHEDULE

16. DISTRIBUTION STATEMENT (of this Report)

Approved for Public Release: Distribution Unlimited

17. DISTRIBUTION STATEMENT (of the abstract entered in Block 20, if different from Report)

18. SUPPLEMENTARY NOTES

Prepared for publication in the Advances in Chemistry Series, Vol. 184, "Interfacial Photoprocesses: Energy Conversion and Synthesis"

19. KEY WORDS (Continue on reverse side if necessary and identify by block number)

Photoelectrochemistry; luminescence; optical energy conversion

LAMBDA sub MAX

20. ABSTRACT (Continue on reverse side if necessary and identify by block number)

The use of luminescent, n-type 5-1000-ppm CdS:Te and 10 ppm-CdS:Ag polycrystalline photoelectrodes as probes of recombination in photoelectrochemical cells is reported. Except for intensity, the emission spectra (λ_{max}, 600-700 nm) are insensitive to the presence of S^{2-}/S_n^{2-} electrolyte and to the excitation wavelengths and electrode potentials employed. With ultraband gap irradiation ($\lambda \leq$ 500 nm) and aqueous

LAMBDA LESS THAN OR =

DD FORM 1 JAN 73 1473 EDITION OF 1 NOV 65 IS OBSOLETE S/N 0102-LF-014-6601

Unclassified

SECURITY CLASSIFICATION OF THIS PAGE (When Data Entered)

380 155

20. Abstract - continued

S^{2-}/S_n^{2-} or Te^{2-}/Te_2^{2-} electrolytes, optical energy is converted to electricity at 0.1-5% efficiency and to luminescence at 0.01-1.0% efficiency; the effects of surface preparation and grain boundaries in determining efficiency are discussed. Increasingly negative bias applied to CdS:Te and CdS:Ag photoanodes increases emission intensity by 15-100% while the photocurrent simultaneously declines to zero. Band gap edge 514.5-nm excitation yields smaller photocurrents and larger but much less potential dependent emission intensity. These results are consistent with the band bending model presently used to describe photoelectrochemical phenomena.

This article has been published: Adv. Chem. Ser. 184, 185 (1980).

The desire to convert optical energy directly into fuels or electricity has led to the rapid development of photoelectrochemical cells (PECs). A typical PEC consists simply of a semiconductor electrode, a counterelectrode,and an electrolyte. The semiconductor is the key element of the PEC, since it serves in the dual capacities of photoreceptor and electrode. Light absorbed by the semiconductor can be channeled into electrochemical processes leading to the aforementioned energy conversions. Although the physics governing photoelectrochemical phenomena has been elegantly reviewed (1,2), a brief description is in order.

Photoelectrochemical events are initiated by ultraband gap photons which, when absorbed by the semiconductor, produce a conduction band electron and valence band hole. The difference between the dark and illuminated electrode is really the difference between ground and excited states, respectively. Figure 1 illustrates this distinction for an n-type semiconductor. Note that the semiconductor bands are bent in parallel; this is a consequence of the mismatch in chemical potentials between the electrolyte (redox potential) and semiconductor (Fermi level). Band bending occurs over a short distance (~1 μ) from the semiconductor-electrolyte interface into the semiconductor bulk and serves to equilibrate the chemical potentials of the two phases. The distance over which band bending occurs is termed the depletion or space-charge region.

Once the semiconductor excited state has been populated, band bending exerts considerable influence over the attendant deactivation processes. In particular, the potential gradient inhibits the recombination of electron-hole pairs and promotes their separation: The conduction band electron migrates to the counter-electrode where it reduces an electroactive electrolyte species, and the valence band hole migrates to the semiconductor-electrolyte interface where it accepts an electron from an electroactive species, thereby oxidizing it. n-Type semiconductors, the most commonly used photoelectrodes, are thus photoanodes and dark cathodes.

A major obstacle to the practical utilization of these concepts is the undesirable oxidation of the n-type semiconductor electrode itself. Typical is the case of CdS which undergoes photoanodic decomposition via equation 1 (3).

$$CdS \xrightarrow{h\nu} Cd^{+2} + S + 2e^{-} \qquad (1)$$

The problem is minimized by choosing electroactive electrolyte species whose oxidation is kinetically rapid enough to quench reaction 1. For example, sulfide (S^{2-}) or polysulfide (S_n^{2-}) electrolytes greatly inhibit the photoanodic dissolution of CdS (4,5,6,7,8). Polysulfide species can be oxidized at the photoanode and simultaneously reduced at the counterelectrode to yield a PEC which exhibits little change in electrolyte or electrode composition, thus permitting the sustained conversion of optical energy to electricity. This concept has been used to construct PECs employing a variety of photoanodes and electrolytes (9-28).

A major thrust of current PEC research is the improvement of energy conversion efficiency. Central to this goal is an understanding of the semiconductor excited state, particularly the extent to which its deactivation routes might be amenable to experimental control. The semiconductor excited state partitions input optical energy into several pathways, as pictured in Figure 2. A broad division into non radiative and radiative relaxation routes is especially convenient.

At least three non-radiative mechanisms for deactivation are known: heat (lattice vibrations), electrode decomposition, and electrolyte redox reactions with corresponding rate constants k_ℓ, k_d, and k_x, respectively. Heat results from the <u>non radiative recombination</u> of photogenerated electron-hole pairs and its role in PECs has not been explored. Electrode decomposition and electrolyte redox reactions are also non radiative but result from <u>separation</u> of electron-hole pairs, as described above. The rate constants k_d and k_x are strongly influenced by

the choice of electrolyte (29,30,31,32). The sum ($k_d + k_x$) is reflected in the current passed in the external circuit, but chemical methods of analysis are required to differentiate between the two current sources. For CdS-based PECs k_d dominates k_x in OH^- electrolyte, whereas the opposite is true in (poly)sulfide media. There are thermodynamic potentials (E_d and E_{redox}) associated with these reactions (29,33,34); however, the significance of kinetics is underscored by the observation that diffusion dependent electrolyte redox processes can compete with electrode localized decomposition. Other experimental factors which can affect k_d and k_x are excitation intensity and electrode potential (1,5,6,33,34).

Against this background we introduce k_r which represents <u>radiative</u> deactivation resulting from electron-hole pair recombination processes. Luminescence is a powerful tool for characterizing excited states, be they organic, organometallic, or solid state in nature. Emissive properties including spectral distribution, lifetime, and quantum yield permit the calculation of rate constants and the assessment of whether a given reaction is possible during the excited state lifetime. Although a vast literature exists for luminescent semiconductors (36,37), very little is known about radiative decay in the context of a PEC. Studies which have been carried out focus on electroluminescence resulting from injection processes at extreme potentials or in strongly oxidizing or reducing media (38-44). These are frequently transient effects and not appropriate for sustained optical energy conversion. One photoluminescence study which pre-dates our work makes use of n- and p-type GaP photoelectrodes (44). Unfortunately, n-GaP is not strongly emissive nor is k_d negligible in the media employed (32); however, some interesting results with p-GaP were obtained during its use as a photocathode for H_2 evolution, and these will be discussed later (44).

What we had hoped to find are electrodes which emit while mimicking the essential features of electrodes used in operating PECs. As shown in Figure 3,

CdS doped with either Te or Ag (CdS:Te, CdS:Ag) acts as just such a dual electrode-emitter. We find that CdS:Te and CdS:Ag are similar to undoped CdS electrodes in their ability to oxidize aqueous (poly)sulfide and (di)telluride species as part of degenerate electrolysis schemes leading to sustained conversion of optical energy to electricity.

Emission from CdS:Te and CdS:Ag involves intraband gap electronic states introduced by the dopant. Tellurium is thought to substitute at S sites and to give rise to states ~0.2 eV above the valence band (45-52). As an isoelectronic dopant, Te is not expected to alter the electrical properties of CdS appreciably. Because it has a smaller electron affinity than S, Te serves as a trap for holes which then can coulombically bind a conduction band electron, thus forming an exciton. The excitonic binding energy is ~0.22 eV so that appreciable exciton concentrations will exist at room temperature. At higher Te doping levels the exciton is thought to be localized over several nearest neighbor Te atoms with a higher binding energy (47,48). Radiative collapse of the exciton produces the observed luminescence. We have used melt-grown, polycrystalline material which is nominally 5-1000 ppm Te.

The mechanism by which CdS:Ag emits is more complex and depends both on the presence of additional impurities and on whether Ag substitutes at Cd sites or interstitially (53-59). Substitution for Cd would make Ag an acceptor and thus partially compensate the material. We have used melt-grown, polycrystalline 10 ppm CdS:Ag, and the resistivity of ~10^3 Ω-cm as compared to ~1 Ω-cm for undoped CdS (and CdS:Te) is consistent with this role for Ag.

In order to exploit the emissive properties of CdS:Te- and CdS:Ag-based PECs, the cell is assembled in the emission compartment of a spectrophotofluorometer. Inclining the photoelectrode at ~45° to both a laser excitation source and the emission detection optics permits the sampling of front surface emission during the course of photoelectrochemical events. Thus, changes in the emission

spectrum (5 nm resolution) and intensity can be monitored in situ. The excitation source is the continuous output of an Ar ion laser. Generally, the incident power was ~1-15 mW which in the ~3 mm dia beam corresponds to intensities of ~14-212 mW/cm^2. All data were obtained with polycrystalline CdS:Te and CdS:Ag samples from Eagle-Picher Industries, Miami, Oklahoma. The grain sizes in the polycrystalline samples are estimated to be 3-8 mm. Preparation and handling of the (poly)sulfide and (di)telluride electrolytes has been described previously and differs in the use of N_2 rather than Ar for purging (6).

As will be described below, the key finding that we have made is that the emission from CdS:Te and CdS:Ag photoelectrodes is a very sensitive probe of recombination processes within the depletion region and hence of the semiconductor excited state. Our results thus far are consistent with the aforementioned band bending arguments used to interpret photoelectrochemical phenomena. Importantly, we present evidence that experimental parameters such as electrode potential, electrolyte and excitation wavelength may be used to manipulate the semiconductor excited state processes and thus influence the course of optical energy conversion.

Results and Discussion

(a) Stability

As a first step in characterizing CdS:Te- and CdS:Ag-based PECs, we wished to determine the extent to which they share mutual electrochemical processes with undoped CdS. All three electrode materials undergo photoanodic dissolution in OH^- electrolyte according to equation (1). Since CdS photoelectrodes are stabilized by (poly)sulfide and (di)telluride electrolytes, we investigated whether CdS:Te and CdS:Ag are rendered stable by these media using variations in electrode weight, surface quality, photocurrent and luminescence as criteria. In the kinetic scheme of Figure 2,we are seeking evidence that $k_x >> k_d$.

The first criterion of stability is met if there is no appreciable weight loss after sufficient current has passed in the external circuit to decompose part or all of the electrode. Data in Table I indicate that this is the case

for CdS:Te and CdS:Ag electrodes in S^{2-}/S_n^{2} and Te^{2-}/Te_2^{2-} electrolytes. The minimal weight losses observed result primarily from chipping of the electrode when it is demounted. All of the experiments listed in Table I were conducted with the electrode at zero or negative bias; under these conditions optical energy is converted to electricity, if the only electrochemistry corresponds to offsetting oxidation and reduction of polychalcogenide species (Figure 3).

A discussion of surface quality should be prefaced with a description of sample preparation. The "as received" polycrystalline samples of CdS:Te and CdS:Ag used in this study were etched in conc. HCl prior to being used as electrodes. This generally has the effect of increasing emission intensity while leaving the spectral distribution intact.

Depending upon the PEC conditions and the sample employed, we see variable degrees of surface damage. At sufficiently high light intensities ($\gtrsim$50 mW/cm^2) and positive voltages ($\gtrsim$-0.3 V vs SCE) in (poly)sulfide electrolytes, we occasionally encounter darkening of CdS:Ag and CdS:Te surfaces. Even avoiding these conditions, though, there is likely some surface reorganization and we sometimes see discolored electrode surfaces. Recent studies of CdSe electrodes in polysulfide electrolyte indicate that substitution of surface Se sites by S occurs (19,60). A similar exchange involving Te is plausible as is another surface reorganization mechanism based on the propensity of CdTe to undergo photoanodic dissolution in (poly)sulfide media via equation 2 (6,9). It is possible that the HCl etch leaves

$$CdTe \xrightarrow{h\nu} Cd^{+2} + Te + 2e^{-} \qquad (2)$$

a Te-rich surface which could then undergo exchange and/or photoanodic decomposition. Consistent with the latter mechanism is the relative lack of surface damage we observe in (di)telluride media. Both CdS and CdTe are known to be stabilized by Te^{2-} and Te^{2-}/Te_2^{2-} electrolytes (6). We find, however, that CdS:Ag exhibits similar properties with regard to surface stability as CdS:Te so that the role of Te is not resolved.

The variation in surface stability is repeated in the temporal characteristics of photocurrent and luminescence. In (poly)sulfide electrolyte nominally identical samples of CdS:Te or CdS:Ag have displayed both stable and unstable photocurrents and emissive properties. Declining photocurrents and emission intensity are usually accompanied by the aforementioned surface deterioration. Certainly one of the disadvantages of the polycrystalline material used in this study is its nonuniformity. In particular, grain boundaries are notorious sources of discontinuous behavior (61). Since we do not know the surface composition of the etched CdS:Te and CdS:Ag electrodes, we are reluctant to make a definitive statement regarding their stability in (poly)sulfide media. It can certainly be argued that the intraband gap states might influence the k_x - k_d competition. We suspect that the samples which yield the most stable properties may have surfaces much like undoped CdS. Doped materials with thse surfaces could still emit, since the bulk of the excitation beam is absorbed beneath the surface. The studies reported here for (poly)sulfide electrolytes have been conducted with samples exhibiting stable, reproducible, photocurrent and emissive properties.

There is less ambiguitiy in (di)telluride electrolyte. We generally see stable photocurrents, emission and surface properties, although at higher intensities there are often slow monotonic declines in photocurrent and luminescence. There is obvious evidence for the competitive oxidation of colorless Te^{2-} to purple Te_2^{2-} or of either Te^{2-} or Te_2^{2-} to Te: at high light intensities the emission is masked by a layer of Te and/or Te_2^{2-} which can be swept away by greater stirring rates. The visual evidence for oxidation of S_n^{2-} is obscured because the emitting electrode and electrolyte are of similar color. However, we have observed yellowing of the initially colorless S^{2-} solutions as S_n^{2-} forms under PEC conditions, Taken as a unit, the data argue strongly for stability of CdS:Te and CdS:Ag in (di)telluride electrolytes; for polysulfide electrolytes sustained photocurrents and minimal weight loss with

these electrodes may be obtained, but there is strong evidence that surface reorganization processes are involved. Experiments designed to clarify the complications observed in (poly)sulfide media are in progress.

(b) Optical Properties

As described in the introduction, the semiconductor excited state is reached by absorption of ultraband gap photons. Undoped CdS has a band gap of ~2.4 eV and hence a fundamental absorption edge at ~520 nm (62). The absorption onset is very sharp because CdS is a direct band gap material. Absorption spectra of single crystal CdS:Te samples have their onset red-shifted due to an absorption shoulder; the effect of increasing Te concentration is to extend this shoulder deeper into the red (46,47,62). Spectra which we have obtained for 100 and 1000 ppm CdS:Te are presented in Figure 4. Although these spectra were obtained from polycrystalline samples, they are at least qualitatively in agreement with the reported single crystal data in shape and color; there is an obvious visual difference, since the yellow undoped CdS becomes orange at 5-100 ppm CdS:Te and red at 1000 ppm CdS:Te. Similarly, 10 ppm CdS:Ag is red and 100 ppm CdS:Ag is brown-black. In effect the shoulder masks the band edge and hence the value E_{BG}, the band gap energy.

What primarily distinguishes CdS:Te and CdS:Ag from undoped CdS is their ability to emit while they serve as electrodes. In Figure 5 we present emission spectra taken at 293°K for 5, 100, 1000 ppm polycrystalline CdS:Te and for 10 ppm polycrystalline CdS:Ag. A systematic study of single crystal, CdS:Te emission spectra has shown that peak position and half-width may be correlated with doping levels in these samples (48). Our results,though uncorrected for detector response,are qualitatively in agreement: the 5 and 100 ppm emission spectra are very similar with a peak maximum at ~600 nm, but there is a definite red shift of the emission maximum to ~650 nm for 1000 ppm CdS:Te. The emission itself varies from yellow-orange to red-orange in passing from the 5, 100 ppm to the 1000 ppm CdS:Te. For CdS:Ag we observe reddish emission and the band maximum appears at ~690 nm.

We were particularly interested in determining whether the PEC environment perturbed the emission spectra of the doped CdS samples. Typical results are

given in Figure 6 which shows a sequence of emission spectra for 5 ppm CdS:Te taken without electrolyte, with polysulfide electrolyte (1M OH^-/1M S^{2-}/1M S) but out of circuit, and in circuit in the same electrolyte at -0.74 V vs. SCE. Note that except for the change in intensity, the emission spectra are essentially identical. We interpret this to mean that the intraband gap states responsible for luminescence are influenced in the same manner as the conduction and valence bands and thus would undergo parallel band bending.

Additional evidence supporting this interpretation is provided by Figure 7. Here the emission of a 100 ppm CdS:Te photoelectrode is recorded at -0.3,-0.8, and -1.0 V vs SCE in polysulfide electrolyte. Again, although the emission intensity changes, the spectrum does not. Application of negative bias to an n-type semiconductor diminishes the amount of band bending; conversely, positive bias increases band bending (1). Invariance of the emission spectrum under conditions where band bending has been altered is thus consistent with parallel behavior between dopant states and the valence and conduction bands. We should also mention that the spectral distribution of emission appears to be independent of excitation wavelength for the laser lines we normally employ: 488.0, 496.5, 501.7 and 514.5 nm.

We have used these wavelengths as the basis of photoaction and excitation spectra, Table II. There is generally a marked decline in photocurrent in passing from what are certainly ultraband gap energies (488.0, 496.5, 501.7 nm) to 514.5 nm. The data in Table II were obtained in optically transparent sulfide electrolyte at -0.4 V vs SCE at roughly equivalent intensities for each of the four wavelengths. Photocurrents from 501.7 nm excitation are ~4.5 to 10 times those resulting from 514.5 nm excitation, Table II. For undoped single crystal CdS the corresponding experiment was reported to yield a similar photocurrent ratio of 7-13 for excitation at these same two wavelengths (5). Therefore, although the aborption spectra of doped and undoped CdS differ (vide supra) the fundamental absorption edge may

have the same wavelength dependence, i.e., the band gaps might be identical. Complete photoaction and excitation spectra must be obtained to clarify this point, however, and such studies are in progress.

By measuring the emission intensity and photocurrent simultaneously, their relationship as a function of wavelength can be examined. Alongside the photocurrent data in Table II are the corresponding emission intensities measured both in and out of circuit. Two general trends are discernible. One is that the emission intensity increases with wavelength and the other is that the in circuit values are substantially lower than out of circuit values except at 514.5 nm where the difference is small.

In the region of what appears to be the band gap, then, there is an inverse relationship between photocurrent and luminescence intensity. The penetration depth of the excitation beam is a significant factor in explaining all of the phenomena we observe. Literature values for undoped CdS and CdS:Te indicate that the 300°K absorptivity, α, at 514 nm is about 10^3 cm^{-1} vs. ~10^4-10^5 cm^{-1} at 502 nm and shorter wavelengths (46,47,62). Electroabsorption measurements on undoped CdS suggest that there should be little variation of α with electrode potential (63). The excited state deactivation rate constants pictured in Figure 2 should be very dependent on position, since band bending decreases with distance from the semiconductor-electrolyte interface. We would a priori predict that electron-hole pairs produced outside the depletion region are more likely to radiatively recombine than those produced within the depletion region which can more readily separate to produce photocurrent. Since a greater fraction of 514.5 nm than ultraband gap light will be absorbed outside the depletion region, the low energy photons should be more effective at yielding emission and less effective at producing photocurrent than ultraband gap photons.

The in and out of circuit trends may also be interpreted in this manner. Taking the electrode out of circuit removes deactivation routes corresponding to electron-hole separation and thus increases the probability for deactivation via the remaining pathways. Since photocurrent is least important as a decay route for 514.5 nm excitation, the difference between in and out of circuit emission should be smallest, as is observed. Although this logic intimates at a direct trade-off between emission and photocurrent, the data in Table II are evidence that this need not be so. The declines in emission intensity with wavelength may well be due to surface traps which promote non radiative electron-hole pair recombination and can be expected to play a more significant role as the penetration depth decreases (64).

One further point concerns the long wavelength extreme. We have actually observed emission out as far as ~540 nm beyond which emission intensity becomes limited by the optical density of the sample. This is possible evidence that the absorption shoulder corresponds to the emitting excited state. If this were the case, then an alternate explanation for the decline of emission intensity with wavelength is simply that the absorption band leading to emission has peaked and fallen. A complete excitation spectrum could reveal the shape of this band, since most of it is buried beneath the direct band gap transition.

(c) Current-Voltage-Emission Properties

Undoubtedly the most significant feature of the luminescent photoelectrodes is the opportunity they afford to examine the interplay of radiative and non-radiative excited state deactivation routes. As described in the introduction, the PEC can be assembled inside the sample chamber of an emission spectrophotofluorometer so that front surface emission may be monitored during PEC operation. A standard three electrode geometry was used in conjunction with a PAR potentiostat which regulates the photoelectrode potential vs. an SCE. A 1.5x 0.9 cm Pt foil served as the counterelectrode. The photoelectrodes were irregularly shaped but often small enough to be completely illuminated by the 3 mm dia laser beam.

Electrodes which were larger than the excitation beam were also used. In this case excitation at a spot on the surface results in emission over the entire sample surface. There are at least three explanations for this. The first is that excitons may migrate and radiatively recombine throughout the sample. We expect exciton diffusion lengths to be small at room temperature, but to our knowledge they have not been measured for CdS:Te and CdS:Ag. We cannot, therefore, rule this out. A second possibility involves re-absorption and re-emission of emitted light enough times to transport it throughout the sample. Since most of the emitted light is not appreciably absorbed by the sample, we think that this, too, is unlikely but still possible. The most plausible explanation, we feel, is simply that the emitted light is scattered to the extent that it emerges throughout the sample. Some role may be played by grain boundaries in this process. In several samples where obvious grain boundaries exist, we find luminescence only within the irradiated grain; emission ceases abruptly at the boundary. In this sense the boundary may be acting as a trap for nonradiative recombination if migration processes are involved or as a reflecting or absorbing surface if scattering is the dominant mechanism. In either case grain boundaries are not a requirement for emission; we have recently obtained single crystals of 100 ppm CdS:Te (vide infra) which exhibit the same emission spectrum and this same phenomenon of global emission from local excitation.

The crucial finding with regard to PECs is that electrode potential influences both photocurrent and luminescence efficiency. A typical set of results is presented in Figure 8 for a 100 ppm CdS:Te photoelectrode and 1M OH^-/1M S^{2-}/0.2M S electrolyte. With 496.5 nm ultraband gap excitation the photocurrent declines with increasingly negative potential, eventually reaching zero at ~-1.1 V vs SCE. Over the same potential range the emission intensity more than doubles! We have chosen the expedient of monitoring emission intensity at the band maximum of 600 nm, since the spectrum is independent of potential (vide supra).

The data presented in Figure 8 is reminiscent of the results presented in the preceding section insofar as emission is concerned. Out of circuit emission values such as those given in Table II should correspond to the emission intensity at zero photocurrent, the point where the current-voltage curve intercepts the voltage axis. Recall that the out of circuit and in circuit values were most similar for 514.5 nm excitation and quite disparate for ultraband gap irradiation. Complete current-voltage-emission data should reflect this relationship.

The direct comparison is afforded by Figure 9 which is based on a 10 ppm CdS:Ag photoelectrode in 1M OH^-/1M S^{2-}/0.2M S electrolyte. Comparable intensities of 496.5 and 514.5 nm excitation result in dramatically different photocurrent-luminescence properties. With respect to photocurrent, ultraband gap 496.5 nm excitation yields substantially larger photocurrents than band gap edge 514.5 nm light. The maximum output voltage for a given intensity E_V, defined as the difference between the voltage at which zero photocurrent obtains and the value of E_{redox}, is ~500 mV for 496.5 nm light and ~320 mV for 514.5 nm excitation from Figure 9. The wavelength dependence of photocurrent and output voltage has been reported for several n-type semiconductor photoelectrodes; larger values for both are obtained with ultraband gap photons than with band gap edge photons because of the different fractions of light absorbed within the depletion region (5,6,10).

As the photocurrent in Figure 9 declines to zero in passing to increasingly negative potentials, the emission intensity increases by up to 50% with 496.5 nm excitation, and drops slightly (~6%) with 514.5 nm excitation. The emission intensities at the two wavelengths of Figure 9 are about the same because the 496.5 nm excitation is slightly more intense after correction for electrolyte absorption. For identical excitation intensities we normally see less luminescence intensity at 496.5 nm than at 514.5 nm (Table II). The dramatic difference in

luminescence intensity with electrode potential at these two wavelengths has been observed by us with all of the electrode materials used and in both sulfide and polysulfide electrolytes. Generally the percentage increase in luminescence in passing to the negative extreme of the current-voltage curve is 15-100% with ultraband gap excitation wavelengths of 488.0, 496.5, and 501.7 nm. Exciting with 514.5 nm yields less than 6% changes and these are often declines. This trend persists even at 514.5 nm light intensities which are sufficiently high to produce photocurrents comparable to those achieved with lower intensity ultraband gap excitation. Again, we ascribe this difference to the smaller fraction of incident light absorbed within the depletion region. Essentially, a greater fraction of light is then absorbed in a region of less band bending, a region where the excited state deactivation rate constants should be more insensitive to changes in electrode potential.

To further probe the generality of this phenomenon, a similar experiment was conducted in ditelluride electrolyte, Figure 10. The electrode is 5 ppm CdS:Te. At comparable incident intensities of 496.5 and 514.5 nm light, approximately 20% and 3% increases in emission intensity occur over the range of -0.7 to -1.2 V vs. SCE, respectively. It would be difficult to predict a priori how the luminescence in ditelluride would differ from that observed in polysulfide. If all of the rate constants of Figure 2 were identical for the two electrolytes, then there should be an exact correspondence between the current-voltage-emission curves. This assertion assumes that CdS:Te and CdS:Ag behave as undoped CdS for which the conduction and valence band energies have been determined to be independent of polychalcogenide electrolyte (6). Of course, the ~0.4 V difference in E_{redox} energies means that output voltages in Te^{2-}/Te_2^{2-} electrolyte will be considerably reduced relative to polysulfide media. Our data thus far indicates similar features for the two electrolytes, but considerably more data needs to be collected before comparisons can be comfortably made.

Although the figures themselves are illustrative, we should comment on the range of conditions employed for which at least two features are noteworthy. First, the kinds of percentage increases in emission which we observe have been obtained at various sweep rates and with point-by-point equilibration. The difference in emission at maximum and near-zero photocurrents is easily observed visually by pulsing the electrode between the appropriate potentials. We also have confidence that the effect is real because it is reproducible either point-by-point or in the reverse sweeping of potential. In some cases we have swept through the potential range many times in succession and still see the same variation in emission and photocurrent.

The other feature of interest is that the different doping levels of CdS:Te and 10 ppm CdS:Ag all show similar effects. We believe that the mechanism by which luminescence occurs is likely different for the two dopants, and it is therefore significant that they exhibit the same kinds of potential and wavelength dependence of emission intensity. This observation leads us to believe that luminescence will be a very general probe of recombination processes in PECs.

(d) Efficiency.

A complete characterization of the semiconductor excited state really requires a detailed energy balance. Although the input optical energy is easily measured with a radiometer, each of the dissipation pathways shown in Figure 2 involves a different technique for its determination. At this point we are able to accurately determine the efficiency of electrochemical redox processes and to estimate the efficiency of luminescence, processes governed by k_x and k_r, respectively. In principle,the efficiency of non radiative recombination could be estimated by difference, assuming that k_ℓ, k_x, and k_r represent the only significant deactivation routes.

For the degenerate electrolysis pictured in Figure 3, the current-voltage curve permits calculation of the efficiency at which optical energy is converted directly to electricity. Since the Pt counterelectrode is at E_{redox}, passage

of photoanodic current at potentials equal to or negative of this value represents optical energy conversion (4). The maximum product of photocurrent and output voltage is the maximum power output, and division by input optical power yields the efficiency, η.

In Table III we have compiled typical efficiencies for CdS:Te and CdS:Ag-based PECs in polysulfide media. Note that, in general, they do not exceed 1% and are therefore significantly lower than the ~5% efficiency observed for ~500 nm monochromatic light with single crystal undoped CdS electrodes (5). We attribute this to both the polycrystallinity of the materials and the surface quality. On occasion we have seen efficiencies which are comparable to the undoped single crystal values; they have been more the exception than the rule, however.

The efficiency is really given by equation (3) where $\Phi_x = k_x/\sum_i k_i$ is

$$\eta = \frac{\Phi_x E_V}{E_{BG}} \qquad (3)$$

the quantum efficiency for electron flow in the external circuit. The maximum value of Φ_x is 1.0; for E_V it is the band gap energy, E_{BG}. Table III reveals that both Φ_x and E_V are at best a tenth of the maximum values and are thus jointly responsible for the poor efficiencies. Much lower efficiency in Te^{2-}/Te_2^{2-} relative to S^{2-}/S_n^{2-} is expected on the basis of less band bending, a result of the more negative value of E_{redox} (-1.1 vs -0.7 V vs SCE).

Determining the luminescence efficiency is difficult because of its spatially diffuse nature. We have employed two techniques for estimating its magnitude. The first method provides an upper limit of emission efficiency by finding physical conditions which produce more intense emission from the same excitation intensity. In agreement with the literature (46,47,48), we have found that simply lowering the temperature to 77°K generally produces such changes. Figure 11 depicts the emission spectral changes resulting from decreasing the temperature. Although the peak position of the 50 ppm CdS:Te sample does not change very much, the peak sharpens and increases

in intensity dramatically. Integration of the peak areas indicates an ~40-fold increase in intensity upon cooling and thus sets an upper limit of 0.025 for emission quantum efficiency at room temperature. Data in Table III show that for the samples examined, maximum values of Φ_r determined in this manner are 0.01-0.10.

We have effectively defined the emission quantum yield as (photons emitted)/(photons absorbed). However, in the context of a PEC an equally satisfying measure would be (energy emitted)/(energy absorbed). The direct interconversion of definitions necessitates integration over the spectral distribution of emitted light. We have sidestepped this problem by using a radiometer with flat wavelength response to sample the emitted light from the back side of a flat electrode. Correcting for the fraction of emitted light sampled and assuming isotropic luminescence, we then typically find values of 0.1-1.0% efficiency for the conversion of input optical energy to emission in electrolytes of (poly)sulfide. This range is certainly consistent with the upper limits set forth in Table III. Therefore, although it is not the dominant pathway, radiative deactivation can be a significant route for energy dissipation for the CdS:Te and CdS:Ag excited states.

The dominant deactivation mechanism is non radiative electron-hole recombination based on the low efficiencies of emission and photocurrent. As was mentioned before, it is this feature which masks the extent to which energy trade-offs exist between luminescence and photocurrent. Figures 8-10 confirm the data of Table II which show that an inverse potential dependence between emission and photocurrent does not always exist. At high excitation intensities we have on occasion seen the emission intensity plateau at negative potentials as shown in Figure 9 or peak and then decline at still more negative potentials. It is intriguing, however, that there is a large potential and hence band bending range over which both photocurrent and emission intensity are relatively constant and that both deviate from this plateau at about the same potential. A complete interpretation of all these observations awaits the evaluation of all of the rate constants of Figure 2.

Summary and Perspective

We believe that the luminescent properties of semiconductor photoelectrodes represent a powerful technique for probing recombination processes in operating PECs. The key finding is that both emission intensity and photocurrent of n-type CdS:Te and CdS:Ag photoelectrodes are influenced by experimental PEC parameters in a manner consistent with band bending arguments commonly used to describe photoelectrochemical phenomena. Increases in emission intensity of ~15-100% with ultraband gap ($\lambda \lesssim 500$ nm) irradiation are observed with increasingly negative potentials; simultaneously, over the same potential range the photocurrents in aqueous S^{2-}/S_n^{2-} or Te^{2-}/Te_2^{2-} electrolytes decline to zero and underscore the significance of the depletion region in determining the relative rates of electron-hole separation and recombination. Simply put, we find that conditions minimizing band bending in CdS:Te and CdS:Ag photoelectrodes lead to increased emission intensity and reduced photocurrents. Ultraband gap photons are more effective at producing photocurrent and less effective at yielding emission than band gap edge 514.5 nm light because a greater fraction is absorbed within the depletion region. It is gratifying to us that two different materials, CdS:Te and CdS:Ag, with different emission spectra and presumably different emissive mechanisms, both give emissive properties corresponding to this simple model.

The polycrystallinity of the melt-grown CdS:Te and CdS:Ag samples and lack of knowledge of their surface composition precludes definitive conclusions regarding their PEC properties relative to those of undoped CdS. However, we have recently made several observations which cast some insight in this direction. First, we have found that etching with Br_2/MeOH leads to vastly superior PEC properties relative to HCl etching (65,66). With respect to Table III, the Br_2/MeOH etchant leads to 3-5% for η_{max} at ~500 nm input light. Output voltages of 0.45 V and quantum

efficiencies for electron flow of 0.25 (at η_{max}) and 0.35 maximum are typical. These values are almost as good as those previously reported for undoped single crystal CdS samples (5,6). Additionally, the Br_2/MeOH treatment leads to greater photocurrent stability and far less surface degradation under comparable PEC conditions (vide supra, Stability).

These observations lead us to believe that the surface produced by HCl etching is the principal source of poor PEC properties. Chemically, Te and Ag are relatively inert to HCl compared to Br_2/MeOH and the former etchant may not produce as uniform a surface. The differences in etchants seem to be real and reproducible--a sample etched with HCl and exhibiting poor current-voltage properties can be etched with Br_2/MeOH to yield good properties and subsequently re-etched with HCl to regenerate the inferior current-voltage curves.

A second observation we have made concerns experiments with single crystal 100 ppm CdS:Te. As described in the section on Optical Properties, the emission spectrum of the single crystal material matches that of the polycrystalline 100 ppm samples and, in fact, the luminescence efficiencies are very similar. The PEC output parameters of the single crystals (Br_2/MeOH etch) are, however, markedly better. For example, we have observed efficiencies of 7.5% (η_{max}), output voltages at η_{max} of 0.60 V, and quantum efficiencies (Φ_e) at η_{max} of 0.45. These values indicate that grain boundaries may exert some influence on output parameters. A more dramatic illustration is our observation that the 15-100% increases in emission intensity with potential seen with polycrystalline 100 ppm CdS:Te become up to 500% increases with single crystal samples! Again, this effect is observed with ultraband gap wavelengths; at 514.5 nm we see the same independence of emission intensity on potential observed with polycrystalline samples.

We would predict that the effect of grain boundaries on PEC properties would be most pronounced if they occur within the depletion or optical penetration regions of the semiconductor. The grain size of 3-8 mm in our polycrystalline samples is

a visual surface measurement and though this dimension is far larger than the 10^{-3}-10^{-2} mm depths relevant to band bending and optical absorption, we have no way of knowing whether grain boundaries exist beneath the surface at these depths. Even beyond these depths, the boundaries may serve as nonradiative recombination sites and quench emission and/or photocurrent. Further studies on the role of grain boundaries are in progress but at this point our observations serve to emphasize the extent to which current-voltage-luminescence properties are independent of sample preparation.

At least one previous effort was made to observe the luminescent phenomena described in this paper, and it illustrates the potential generality of the technique. Memming and Beckmann studied photocathodic evolution of H_2 from p-GaP electrodes in acid medium (44). They sought evidence for the quenching of photoluminescence by the passage of photocurrent but found differences in emission intensity of only a few percent over the potential range examined. A more sensitive differential luminescence technique confirmed their observation. Although p-GaP, like the CdS:Te and CdS:Ag samples used here, is unusual with respect to the intensity of emitted light, there is no reason why more weakly emitting photoelectrodes should not be examined. Many of the materials now commonly used in PEC studies are either luminescent at room temperature or may be doped to induce emission as has been done with CdS.

Care must be exercised in extending results for doped semiconductor photoelectrodes to undoped systems. We are encouraged by the insensitivity of the emission spectra of CdS:Te and CdS:Ag to a variety of experimental conditions including the excitation wavelength, the electrode potential, and the presence of S^{2-}/S_n^{2-} electrolyte. We feel that this is strong evidence that the dopant induced states and valence and conduction bands all undergo parallel band bending. It is possible that the dopant states can influence interfacial electron transfer processes, but more systems need to be examined to determine how important this effect will be. We feel, however, that at this point there are enough correlations

between the doped and undoped CdS-based PECs to make the pursuit of these systems worthwhile.

Acknowledgment. It is a pleasure to thank the Office of Naval Research, the Research Corporation, and the University of Wisconsin-Madison Graduate School Research Committee for financial support of this work. We also wish to acknowledge many helpful discussions with Professor John Wiley of the UW-Madison Electrical Engineering Department.

Table I. Stability of n-type CdS:Te and CdS:Ag Photoelectrodes in Aqueous Polychalcogenide Electrolytes.[a]

Electrode[b]	Electrolyte[c]	Electrode(mol x 10^4) Before	After	Electrons (mol x 10^4)	Avg.i, mA	Time,h	Source[d]
CdS:Te 1000 ppm	S_n^{2-}	0.847	0.820	1.73	0.069	67.2	Hg
CdS:Ag 10 ppm	S_n^{2-}	1.87	1.70	5.14	0.117	117.8	Hg
CdS:Te 100 ppm	S_n^{2-}	136.7	136.7	5.17	0.066	210.0	Hg
CdS:Ag 10 ppm	Te_n^{2-}	1.27	1.26	1.31	0.086	40.8	Xe
CdS:Te 100 ppm	Te_n^{2-}	9.36	8.75[e]	3.96	0.259	41.0	Xe

[a]Photoelectrochemical cell with the indicated electrode as photoanode. For the experiments in S_n^{2-} electrolyte, a power supply was used as the load, cf. Figure 3. For CdS:Ag in Te_n^{2-} electrolyte, a third,reference electrode was also used in conjunction with a potentiostat. Pt foil served as the counterelectrode in all cases.

[b]Electrodes were etched in conc. HCl prior to use. They are melt-grown, polycrystalline samples from Eagle-Picher Industries. The CdS:Te and CdS:Ag specimens have resistivities of ~1 and 2000 ohm-cm, respectively, and were used in irregular shapes.

[c]Electrolyte is 1M OH^-/1M S^{2-}/0.2M S (S_n^{2-}) or 5M KOH/0.05M Te^{2-}/0.01 M Te_2^{2-} (Te_n^{2-}). The polysulfide electrolyte was purged with N_2 and the electrode was held at ~-0.05 V vs the counterelectrode; the negative lead of the power supply was connected to the photoelectrode. Several of the experiments in S_n^{2-} were periodically interrupted to renew the electrolyte, since even with N_2 purging there is slow decomposition from impurities. For the CdS:Ag experiment in Te_n^{2-}, the photoelectrode was held at -1.04 V vs SCE, the value measured for E_{redox}; the CdS:Te experiment in Te_n^{2-} was run at 0.00 V vs the counterelectrode.

[d]Hg is a uv-filtered 200 W super high pressure Hg arc lamp; Xe is an unfiltered 150 W Xe lamp.

[e]Crystal chipped badly upon demounting and not all of it could be recovered.

Table II. Wavelength Dependence of Emission and Photocurrent[a]

Electrode[b]	λ, nm	Relative Emission Intensity, a.u.[c] Out of Circuit	In Circuit	Photocurrent, μA[d]
1. CdS:Te 5 ppm	514.5	235	232	12
	501.7	187	147	85
	496.5	147	106	84
	488.0	116	88	72
2. CdS:Te 1000 ppm	514.5	300	295	5
	501.7	310	281	22
	496.5	236	204	28
	488.0	187	158	34
3. CdS:Ag 10 ppm	514.5	1623	1612	38
	501.7	355	305	395
	496.5	227	170	347
	488.0	158	115	287

[a]The experiments were conducted in optically transparent 1M OH^-/1M S^{2-} electrolyte with the electrodes at -0.4 V vs SCE. At this potential the photocurrent is saturated with respect to potential. Electrodes were excited by an ~3 mm dia Ar ion laser beam of ~3 mW.

[b]Electrodes are irregularly shaped. The surface area exposed to the electrolyte is 0.15, 0.075 and 0.18 cm^2 for electrodes 1, 2 and 3, respectively. The fraction of the electrode illuminated can be estimated by dividing these numbers into 0.071 cm^2, the laser beam area.

[c]Relative emission intensity was measured with a flat wavelength response radiometer which was filtered to eliminate the exciting wavelengths and positioned to sample front surface electrode emission. A switch on the PAR potentiostat permitted the PEC to be brought in and out of circuit without disturbing the geometry. For a given electrode experimental conditions are identical except for the exciting wavelength. The emission values have been corrected to the same number of einsteins/sec at each wavelength; however, values between electrodes cannot be compared because different geometries and light intensities were employed.

[d]Photocurrents have been corrected for each electrode to equivalent einsteins/sec. For a given electrode experimental conditions are identical except for the exciting wavelength. Values between electrodes are not comparable; cf. footnote c.

Table III. Energy Conversion Characteristics[a]

Property	CdS:Te, CdS:Ag-based PEC[b]	Undoped CdS-based PEC[b]
η_{max} [c]	0.1-1.0 %	3-7 %
E_V @ η_{max} [d]	0.20-0.30 V	0.3-0.4 V
Φ_x @ η_{max} [e]	0.01-0.05	0.3-0.5
Φ_x max [f]	0.1	0.8-1.0
Lum. η [g]	0.1-1.0 %	———
Φ_r(max) [h]	0.01-0.10	———

[a]Measures of efficiency for the conversion of $\lesssim$10 mW/cm^2, ~500 nm monochromatic input optical energy to electricity and/or luminescence in aqueous polysulfide media. Listed values are meant to be representative.

[b]The indicated electrodes serve as the photoanodes of a PEC like that shown in Figure 3. Data were also obtained with a third, reference electrode and a potentiostat. Undoped CdS data were taken from Refs. 5,6. All measurements were made with samples etched in conc. HCl.

[c]Maximum efficiency for the conversion of optical energy to electricity. Obtained from current-voltage curves like those shown in Figures 8-10 by maximizing the product of output voltage (cf. text and footnote d) and photocurrent, then dividing by input optical power.

[d]Output voltage at maximum efficiency. The output voltage is the absolute value of the difference between the electrode potential on the current-voltage curve and E_{redox}. For the two electrode cell shown in Figure 3, E_V is the electrode potential, since 0.0 V is E_{redox} (4).

[e]Φ_x is the quantum yield for electron flow in the external circuit, measured here at the potential corresponding to maximum efficiency.

Table III. continued

[f]The maximum value of Φ_x, usually measured at up to 0.5 V positive of E_{redox} where the photocurrent is saturated with respect to potential.

[g]Efficiency for the conversion of optical energy to luminescence, defined here as (Energy emitted)/(Energy absorbed). A flat wavelength response radiometer is used to estimate the energy emitted, cf. text.

[h]Estimated maximum emission quantum efficiency, defined as $k_r/\sum_i k_i$ and as (photons emitted)/(photons absorbed). Low temperature emission spectra of unmounted CdS:Te and CdS:Ag were used for this estimate, see Figure 11 and text.

Figure Captions

Figure 1. (a) Representation of the dark semiconductor electrode corresponding to the ground state; (b) Irradiation of the electrode produces the excited state which is deactivated here by redox reactions. E_F and E_{BG} are the Fermi level and semiconductor band gap, respectively. E_{redox} is the electrolyte redox potential. Band bending characteristic of the depletion region formed at the *n*-type semiconductor-electrolyte interface is also shown.

Figure 2. Excited state deactivation pathways of the semiconductor electrode. Wavy arrows signify non-radiative decay routes: k_ℓ, k_d, and k_x correspond to electron-hole recombination leading to heat, electron-hole separation leading to photoanodic decomposition, and electron-hole separation leading to electrolyte redox reactions, respectively. The straight arrow and k_r correspond to radiative recombination, the source of luminescence. E_d is the thermodynamic potential for anodic decomposition. Intraband gap states and defects which might play a role in the various deactivation routes have been omitted for simplicity.

Figure 3. A photoelectrochemical cell (PEC) employing n-type CdS:Te or CdS:Ag photoelectrodes luminesces as it converts optical energy to electricity via a degenerate electrolysis reaction. Polychalcogenide electrolytes have been chosen to minimize photoanodic decomposition of the electrode.

Figure 4. Optical density of polycrystalline 100 ppm CdS:Te (squares) and 1000 ppm CdS:Te (circles). Thicknesses are 2.0 and 2.2 mm, respectively, and samples have been polished with 1 micron alumina. The "x" is a literature value optical density of a 2 mm thick, undoped, polished CdS single crystal (5).

Figure 5. Typical 295°K emission spectra of 5, 100, 1000 ppm CdS:Te and 10 ppm CdS:Ag. The CdS:Te samples were excited at 488.0 nm and the CdS:Ag sample at 514.5 nm. Spectra are uncorrected.

Figure 6. Uncorrected emission spectra of 5 ppm CdS:Te in various environments but in a fixed geometry relative to the 488.0 nm laser excitation source and emission detection optics. For curve A no electrolyte was present; curves B and C were both taken with the electrode immersed in 1M OH^-/1M S^{2-}/1M S polysulfide electrolyte but out of circuit and in circuit at -0.74 V vs SCE, respectively. The sharp intensity drop from A to B and C is the result of electrolyte absorption; baseline is not preserved at the high energy end of the emission spectrum due to overlap with the tail of the excitation line.

Figure 7. Uncorrected emission spectra of a 100 ppm CdS:Te electrode at several potentials in 1M OH^-/1M S^{2-}/0.2M S electrolyte. Curves A, B, and C correspond to identical experimental conditions except for electrode potentials of -0.3, -0.8, and -1.0 V vs SCE, respectively. The excitation wavelength is 496.5 nm.

Figure 8. Dependence of photocurrent (solid line and left hand scale) and relative emission intensity (dotted line and right hand scale; monitored at 600 nm) on electrode potential for a 100 ppm CdS:Te-based PEC employing 1M OH^-/1M S^{2-}/0.2M S electrolyte. The photoelectrode was excited with ~ 4 mW of 496.5 nm light. Both measurements were made simultaneously at a sweep rate of 13 mV/sec starting at -0.3 V vs SCE. Electrolyte redox potential is -0.70 V vs SCE. The 3 mm dia laser beam only filled part of the irregularly shaped 0.54 cm^2 electrode surface.

Figure 9. Photocurrent (left hand scale and solid lines) and relative emission intensity (right hand scale and dotted lines) as a function of electrode potential for a 10 ppm CdS:Ag-based PEC in 1M OH^-/1M S^{2-}/0.2M S electrolyte. Experimental conditions in the top and bottom figures are identical except that ~15 mW of 496.5 nm light was used in the former and ~11 mW of 514.5 nm light in the latter. Emission intensity in both cases was monitored at 670 nm; the points labelled "100" on the relative emission intensity scales are about the same absolute intensity. Photocurrent and emission intensity measurements were made simultaneously at a sweep rate of 13 mV/sec starting at -0.3 V vs SCE. The

electrolyte redox potential is -0.70 V vs. SCE. Electrode surface area exposed to the electrolyte is ~0.21 cm^2 and only partially filled by the 3 mm dia laser beam.

Figure 10. Photocurrent (left hand scale and filled circles) and relative emission intensity (right hand scale and open circles) as a function of electrode potential for a 5 ppm CdS:Te electrode in 5M KOH/0.05M Te^{2-}/0.01M Te_2^{2-} electrolyte. Emission intensity was monitored with a flat response radiometer suitably filtered to eliminate the excitation lines of 496.5 nm (top figure) and 514.5 nm (bottom figure). The emission intensity point labelled "100" on the top figure is approximately one-half the value of "100" on the bottom figure. Excitation intensities are comparable at ~10 mW. The electrolyte redox potential is -1.04 V vs. SCE. Electrode surface area exposed to the electrolyte is ~0.12 cm^2 and about half filled by the 3 mm dia laser beam.

Figure 11. Uncorrected emission spectra of 50 ppm CdS:Te at 77°K (solid line) and 295°K (dotted line; ten times scale expansion). The sample was excited with identical intensities of 488.0 nm light at the two temperatures.

Literature Cited

1. Gerischer H. J. Electroanal. Chem., 1975, 58, 263.
2. Gerischer H., "Physical Chemistry: An Advanced Treatise", Vol. 9A, Eyring H., Henderson D., Jost W., Eds. Academic, New York, 1970, Ch.5.
3. Williams, R. J. Chem. Phys., 1960, 32, 1505.
4. Ellis A.B.; Kaiser S.W.; Wrighton M.S. J. Amer. Chem. Soc., 1976, 98, 1635.
5. Ellis A.B.; Kaiser S.W.; Wrighton, M.S. ibid., 1976, 98, 6855.
6. Ellis A.B.; Kaiser S.W.; Bolts J.M.; Wrighton M.S. ibid., 1977, 99, 2839.
7. Hodes G.; Manassen J.; Cahen D. Nature (London), 1976, 261, 403.
8. Miller B.; Heller A. ibid., 1976, 262, 680.
9. Ellis A.B.; Kaiser S.W.; Wrighton M.S. J. Am. Chem. Soc., 1976, 98, 6418.
10. Ellis A.B.; Bolts J.M.; Kaiser S.W.; Wrighton M.S. ibid., 1977, 99, 2848.
11. Heller A.; Chang K.C.; Miller B. J. Electrochem. Soc., 1977, 124, 697.
12. Chang K.C.; Heller A.; Schwartz B.; Menezes S.; Miller B. Science, 1977, 196, 1097.
13. Ellis A.B.; Bolts J.M.; Wrighton, M.S. J. Electrochem. Soc., 1977, 124, 1603.
14. Legg K.D.; Ellis A.B.; Bolts J.M.; Wrighton M.S. Proc. Nat. Acad. Sci. U.S.A., 1977, 74, 4116.
15. Bolts J.M.; Ellis A.B.; Legg K.D.: Wrighton M.S. J. Am. Chem. Soc., 1977, 99, 4826.
16. Miller B.; Heller A.; Robbins M.; Menezes S.; Chang K.C.; Thomson, Jr. J. J. Electrochem. Soc., 1977, 124, 1019.
17. Manassen J.; Hodes G.; Cahen D. ibid., 1977, 124, 532.
18. Noufi R.N.; Kohl P.A.; Bard A.J. ibid., 1978, 125, 375.
19. Heller A.; Schwartz G.P.; Vadimsky R.G.; Menezes S.; Miller B. ibid., 1978, 125, 1156.
20. Hodes G.; Manassen J.; Cahen D. J. Appl. Electrochem., 1977, 7, 181.
21. Tsuiki M.; Ueno Y.; Nakamura T.; Minoura H. Chem. Lett., 1978, 289.

22. Minoura H.; Nakamura T.; Ueno Y.; Tsuiki M. ibid., 1977, 913.

23. Minoura H.; Tsuiki M., Oki T. Ber. Bunsenges. Phys. Chem., 1977, 81, 588.

24. Owen J.R. Nature (London), 1977, 267, 504.

25. Tributsch H. Ber. Bunsenges. Phys. Chem., 1977, 81, 361.

26. Tributsch H. ibid., 1978, 82, 169.

27. Tributsch H. J. Electrochem. Soc., 1978, 125, 1086.

28. Tributsch H.; Bennett J.C. J. Electroanal. Chem., 1977, 81, 97.

29. Memming R. Ber. Bunsenges. Phys. Chem., 1977, 81, 732.

30. Fujishima A.; Inoue T.; Watanabe T.; Honda K. Chem. Lett., 1978, 357.

31. Inoue T.; Watanabe T.; Fujishima A.; Honda K.; Kohayakawa K. J. Electrochem. Soc., 1977, 124, 719.

32. Madou M.; Cardon F.; Gomes W.P. Ber. Bunsenges. Phys. Chem., 1977, 81, 1186.

33. Bard A.J.; Wrighton M.S. J. Electrochem. Soc., 1977, 124, 1706.

34. Gerischer H. J. Electroanal. Chem., 1977, 82, 133.

35. Fujishima A.; Inoue T.; Watanabe T.; Honda K. Chem. Lett., 1978, 357.

36. Leverenz H.W. "An Introduction to Luminescence of Solids," John Wiley and Sons, Inc., New York, 1950.

37. Aven M.; Prener J.S., Eds. "Physics and Chemistry of II-VI Compounds", North Holland Publishing Co., Amsterdam, 1967.

38. Gerischer H. J. Electrochem. Soc., 1978, 125, 218C.

39. Pettinger B.; Schöppel H.-R.; Gerischer H. Ber. Bunsenges. Phys. Chem., 1976, 80, 845.

40. Van Ruyven, L.J.; Williams F.E. Phys. Rev. Lett., 1966, 16, 889.

41. Pettinger B.; Schöppel H.-R.; Yokoyama T.; Gerischer H. Ber. Bunsenges. Phys. Chem., 1974, 78, 1024.

42. Noufi R.N.; Kohl P.A.; Frank S.N.; Bard A.J. J. Electrochem. Soc., 1978, 125, 246.

43. Memming R. J. Electrochem Soc., 1969, 116, 786.

44. Beckmann K.H.; Memming R. ibid., 1969, 116, 368.

45. Aten A.C.; Haanstra J.H. Phys. Lett., 1964, 11, 97.

46. Aten A.C.; Haanstra J.H.; deVries H. Phillips Res. Rept., 1965, 20, 395.

47. Cuthbert J.D.; Thomas D.G. J. Appl. Phys., 1968, 39, 1573.

48. Roessler D.M. ibid., 1970, 41, 4589.

49. Cruceanu E.; Dimitrov A. Sov. Phys. Sol. St., 1969, 11, 1389.

50. Goede O.; Nebauer E. Phys. Stat. Sol. A., 1971, 7, K85.

51. Nebauer E.; Lautenbach J. Phys. Stat. Sol. B., 1971, 48, 657.

52. Cuthbert J.D. J. Appl. Phys., 1971, 42, 739.

53. Colbow K.; Yuen K. Can. J. Phys., 1972, 50, 1518.

54. Brown M.R.; Cox A.F.J.; Shand W.A.; Williams J.M. J. Luminescence, 1970, 3, 96.

55. Woodbury H.H. J. Appl. Phys., 1965, 36, 2287.

56. Klick C.C. J. Opt. Soc. Amer., 1951, 41, 816.

57. Lambe J.; Klick C.C. Phys. Rev., 1955, 98, 909.

58. Vydyanath H.R.; Kröger F.A. J. Phys. Chem. Solids, 1975, 36, 509.

59. Kröger F.A.; Vink J.H.; Vanden Boomgaard Z. Phys. Chem., 1969, 203, 1.

60. Gerischer H.; Gobrecht J. Ber. Bunsenges. Phys. Chem., 1978, 82, 520.

61. Tanenbaum M. in "Semiconductors", Hannay N.B., Ed. ACS Monograph Ser. No. 140, Reinhold Publ. Corp., New York, 1959, Ch. 3.

62. Dutton D. Phys. Rev., 1958, 112, 785.

63. Blossey D.F.; Handler P. in "Semiconductors and Semimetals," Vol. 9, Willardson R.K.; Beer A.C., Eds. Academic Press, New York, 1972, Ch. 3.

64. Bube R.H. "Photoconductivity of Solids," John Wiley & Sons, Inc., New York, 1960, 273-324.

65. Ellis A.B.; Karas B.R. J. Amer. Chem. Soc., 1979, 101, 0000.

66. Ellis A.B.; Karas B.R. to be published.

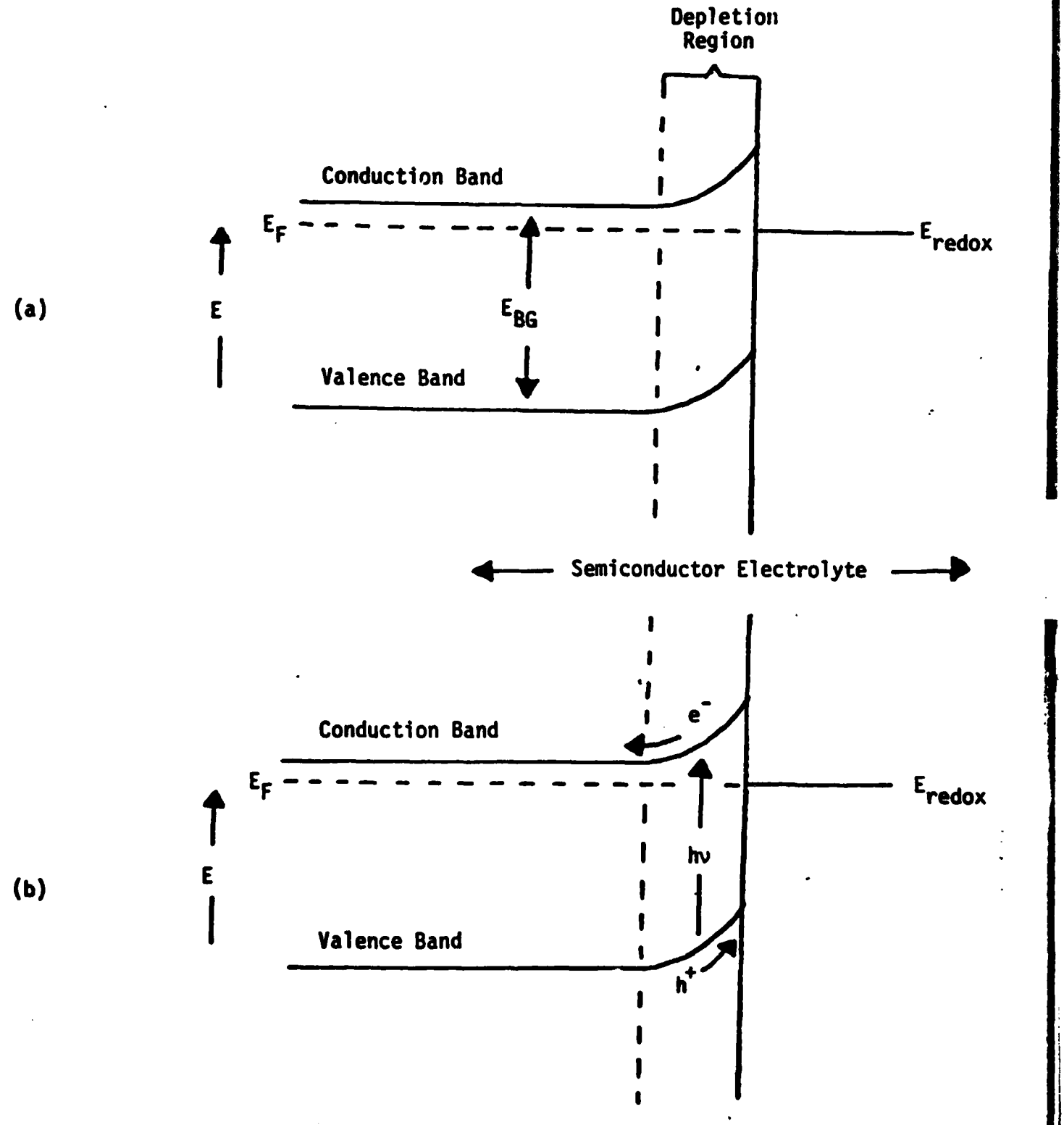
Depletion Region
Conduction Band
E_F
E_{redox}
(a)
E
E_{BG}
Valence Band
Semiconductor Electrolyte
e^-
Conduction Band
E_F
E_{redox}
hν
(b)
E
Valence Band
h^+

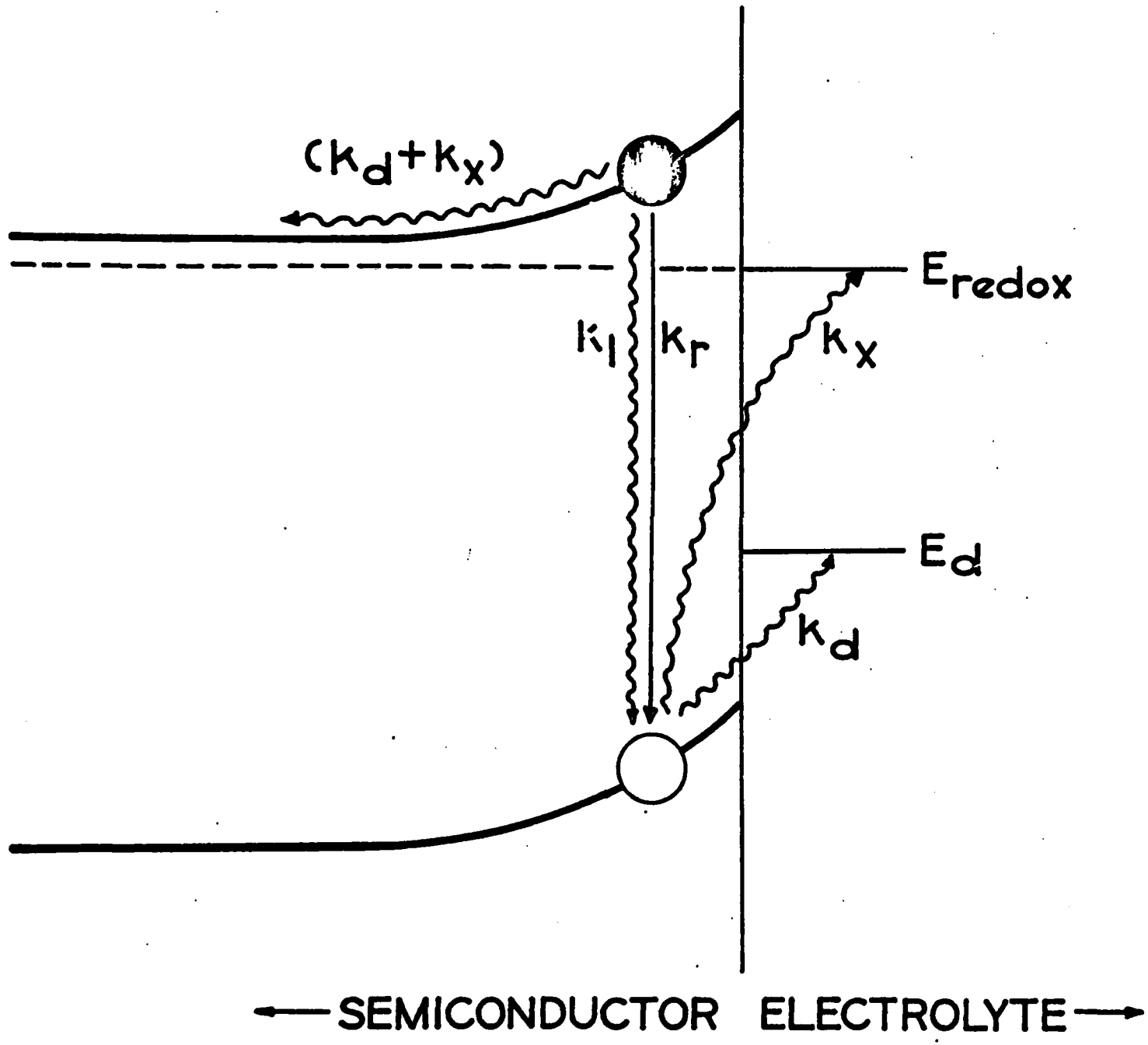
(k_d+k_x)
E_{redox}
k_l
k_r
k_x
E_d
k_d
SEMICONDUCTOR ELECTROLYTE

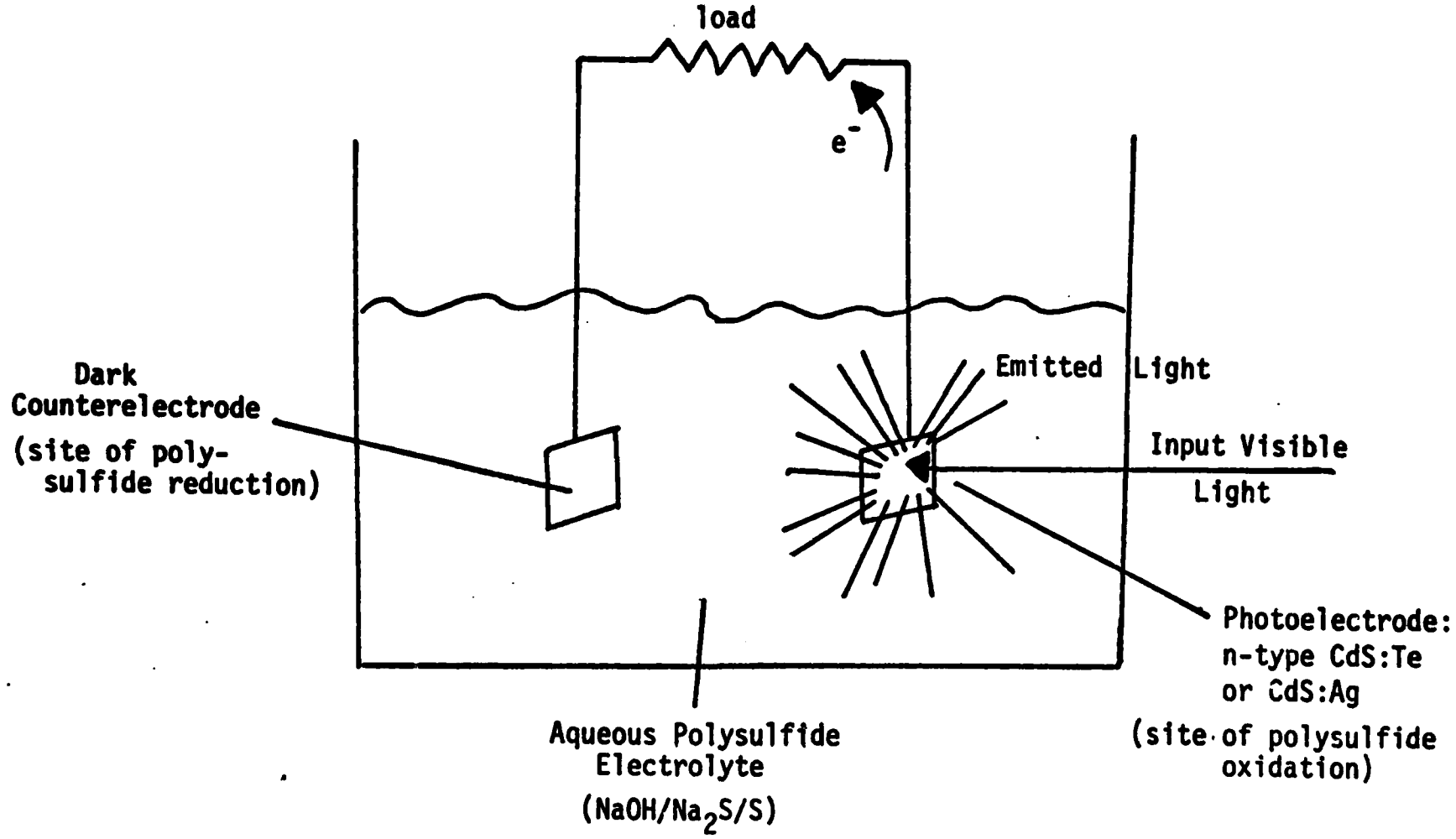
load
e⁻
Dark
Counterelectrode
(site of poly-
sulfide reduction)
Emitted Light
Input Visible
Light
Photoelectrode:
n-type CdS:Te
or CdS:Ag
(site of polysulfide
oxidation)
Aqueous Polysulfide
Electrolyte
(NaOH/Na2S/S)

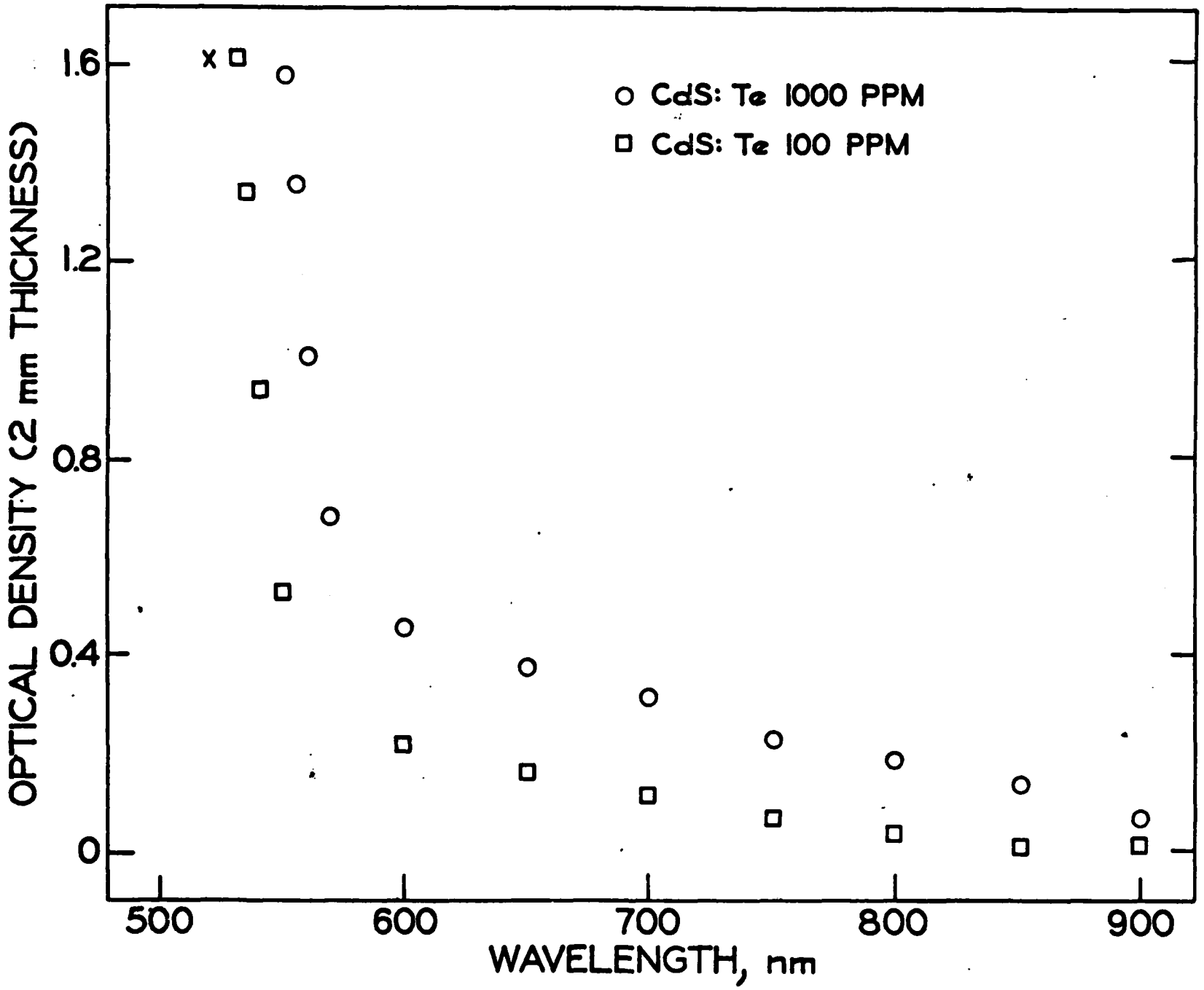
OPTICAL DENSITY (2 mm THICKNESS)
1.6
1.2
0.8
0.4
0
500
600
700
800
900
WAVELENGTH, nm
CdS: Te 1000 PPM
CdS: Te 100 PPM

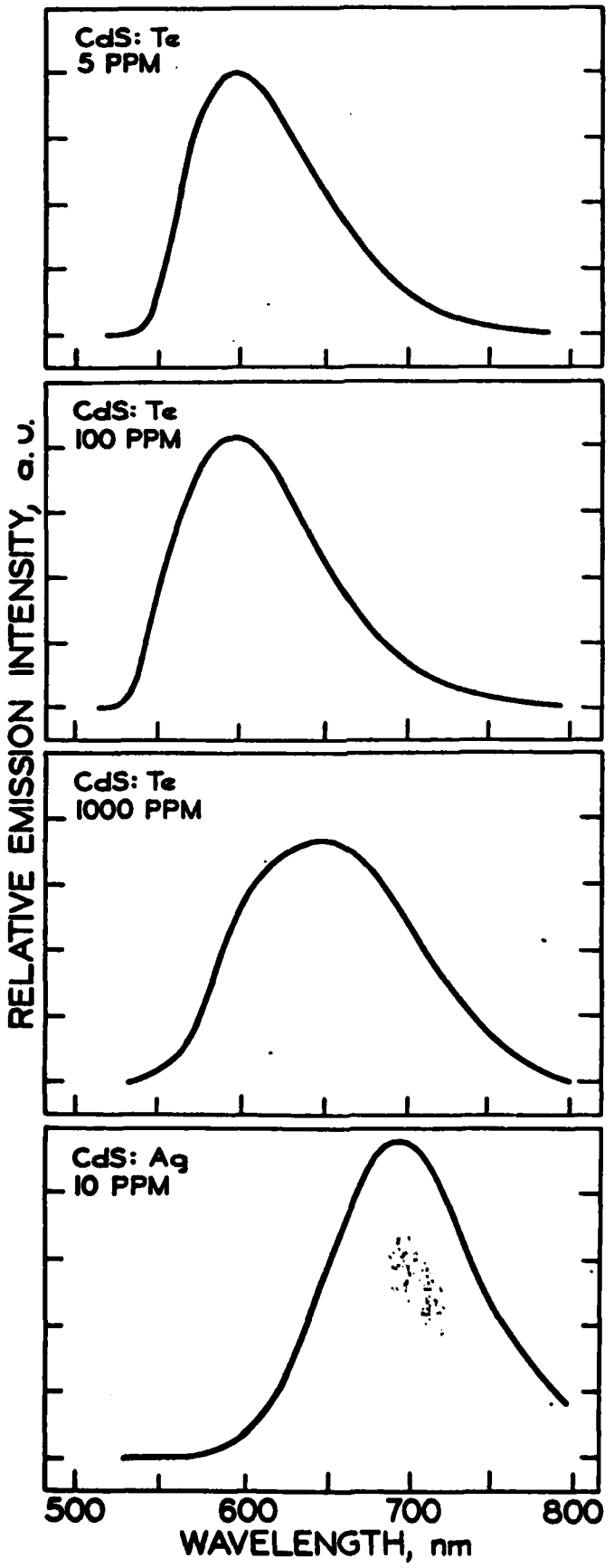
CdS: Te
5 PPM
CdS: Te
100 PPM
CdS: Te
1000 PPM
CdS: Ag
10 PPM
RELATIVE EMISSION INTENSITY, a.u.
500
600
700
800
WAVELENGTH, nm

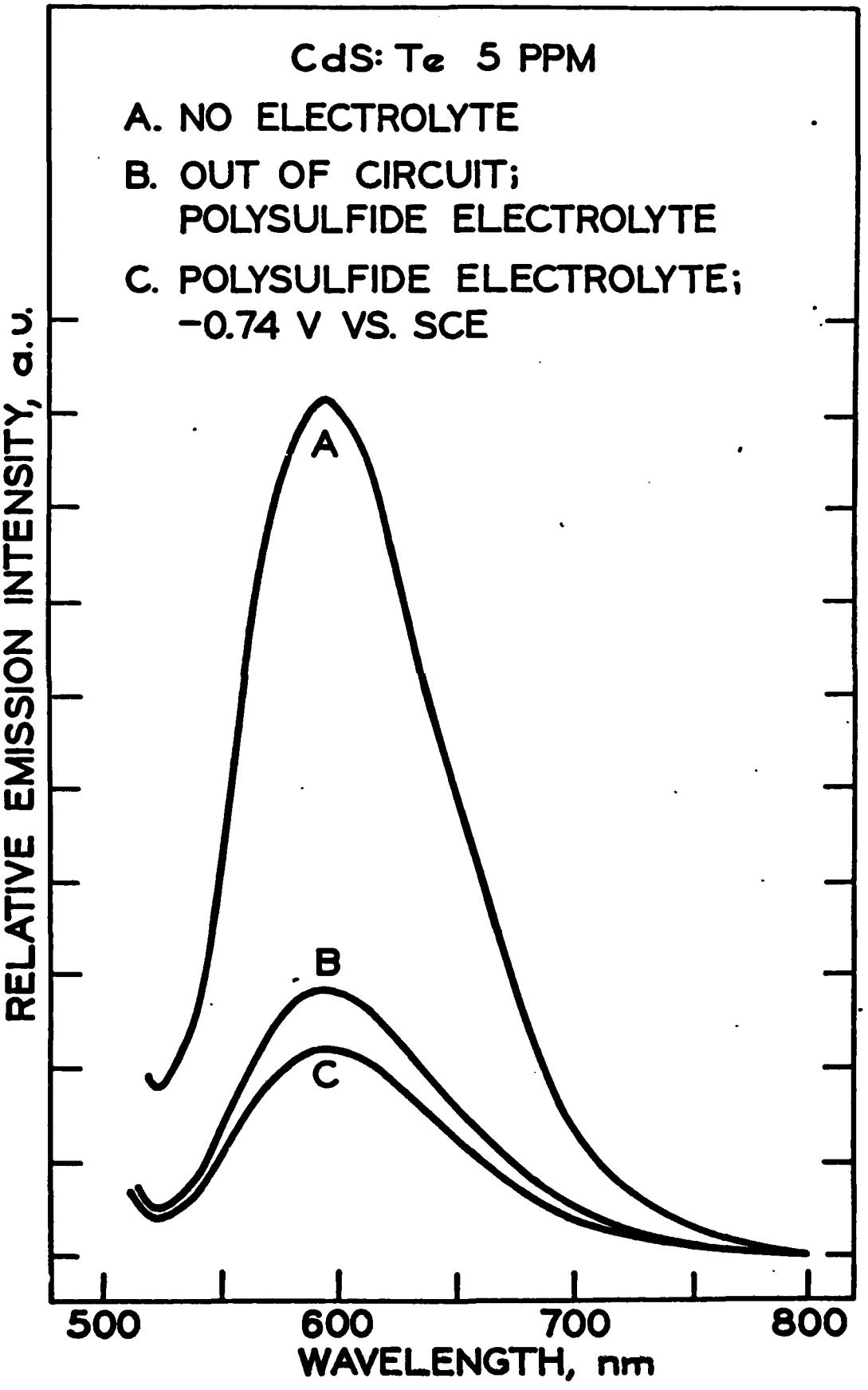
CdS: Te 5 PPM
A. NO ELECTROLYTE
B. OUT OF CIRCUIT;
POLYSULFIDE ELECTROLYTE
C. POLYSULFIDE ELECTROLYTE;
−0.74 V VS. SCE
RELATIVE EMISSION INTENSITY, a.u.
A
B
C
500
600
700
800
WAVELENGTH, nm

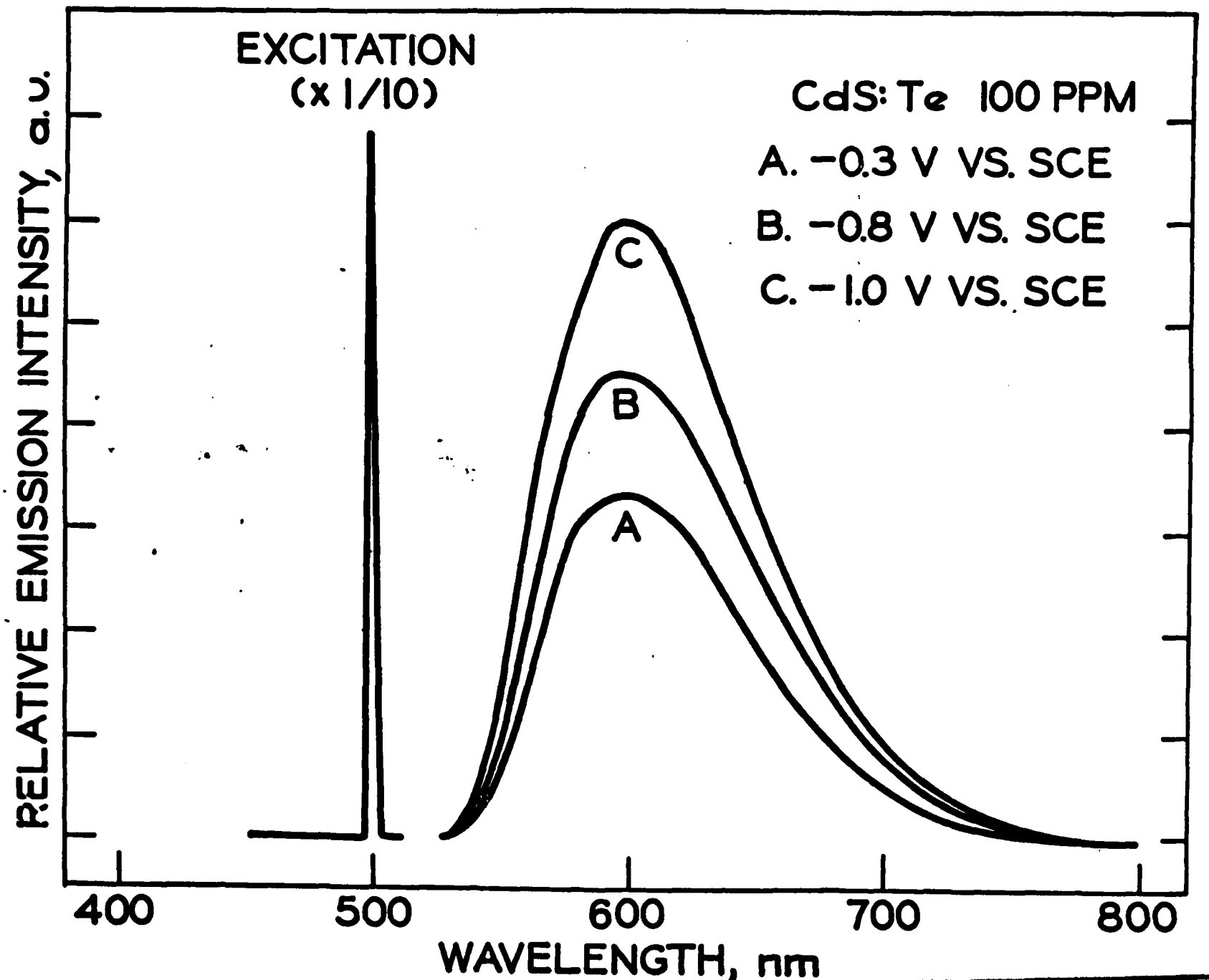
EXCITATION
(x 1/10)
CdS: Te 100 PPM
A. −0.3 V VS. SCE
B. −0.8 V VS. SCE
C. −1.0 V VS. SCE
C
B
A
RELATIVE EMISSION INTENSITY, a.u.
400
500
600
700
800
WAVELENGTH, nm

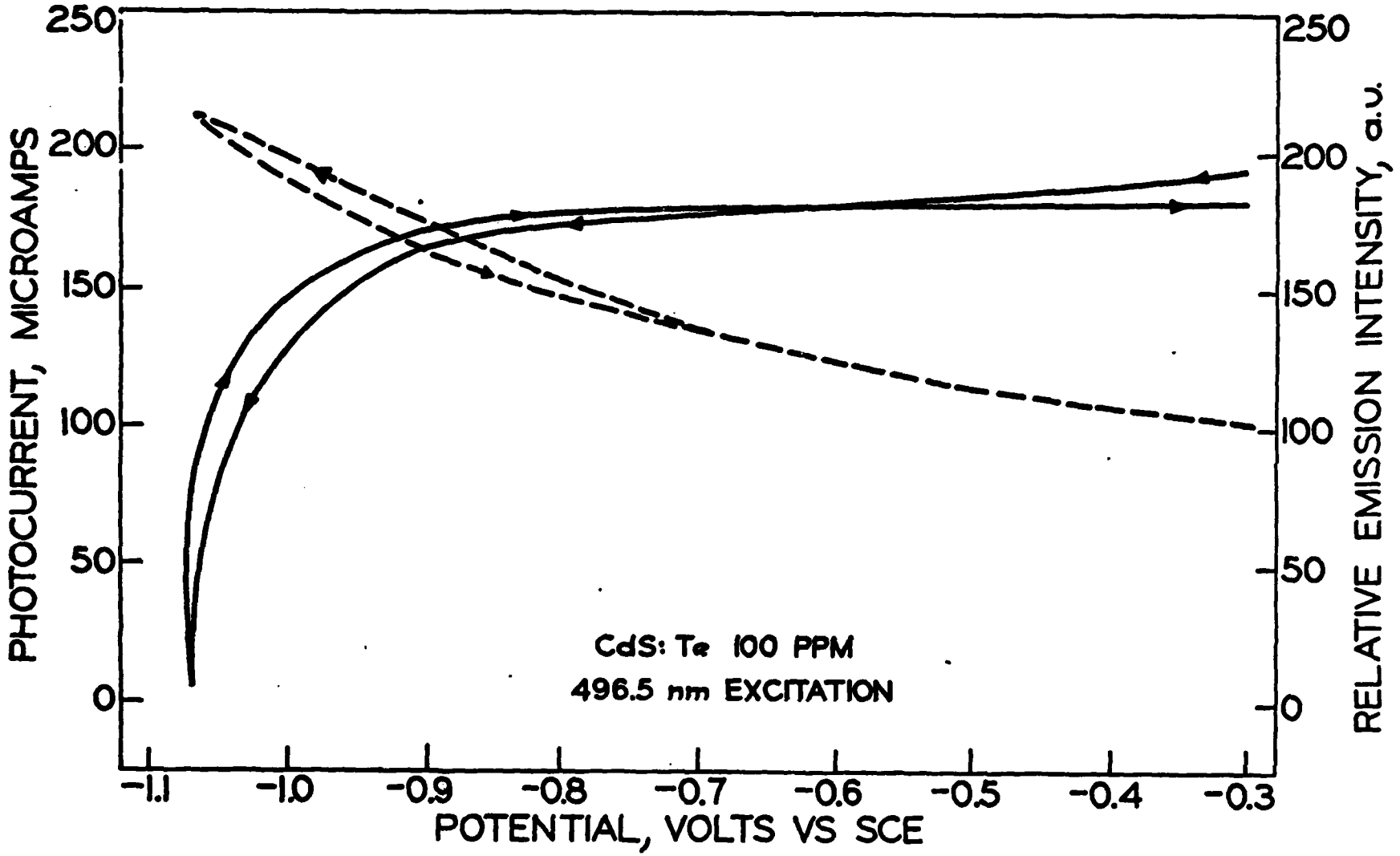
250
200
150
100
50
0
PHOTOCURRENT, MICROAMPS
250
200
150
100
50
0
RELATIVE EMISSION INTENSITY, a.u.
CdS: Te 100 PPM
496.5 nm EXCITATION
-1.1
-1.0
-0.9
-0.8
-0.7
-0.6
-0.5
-0.4
-0.3
POTENTIAL, VOLTS VS SCE

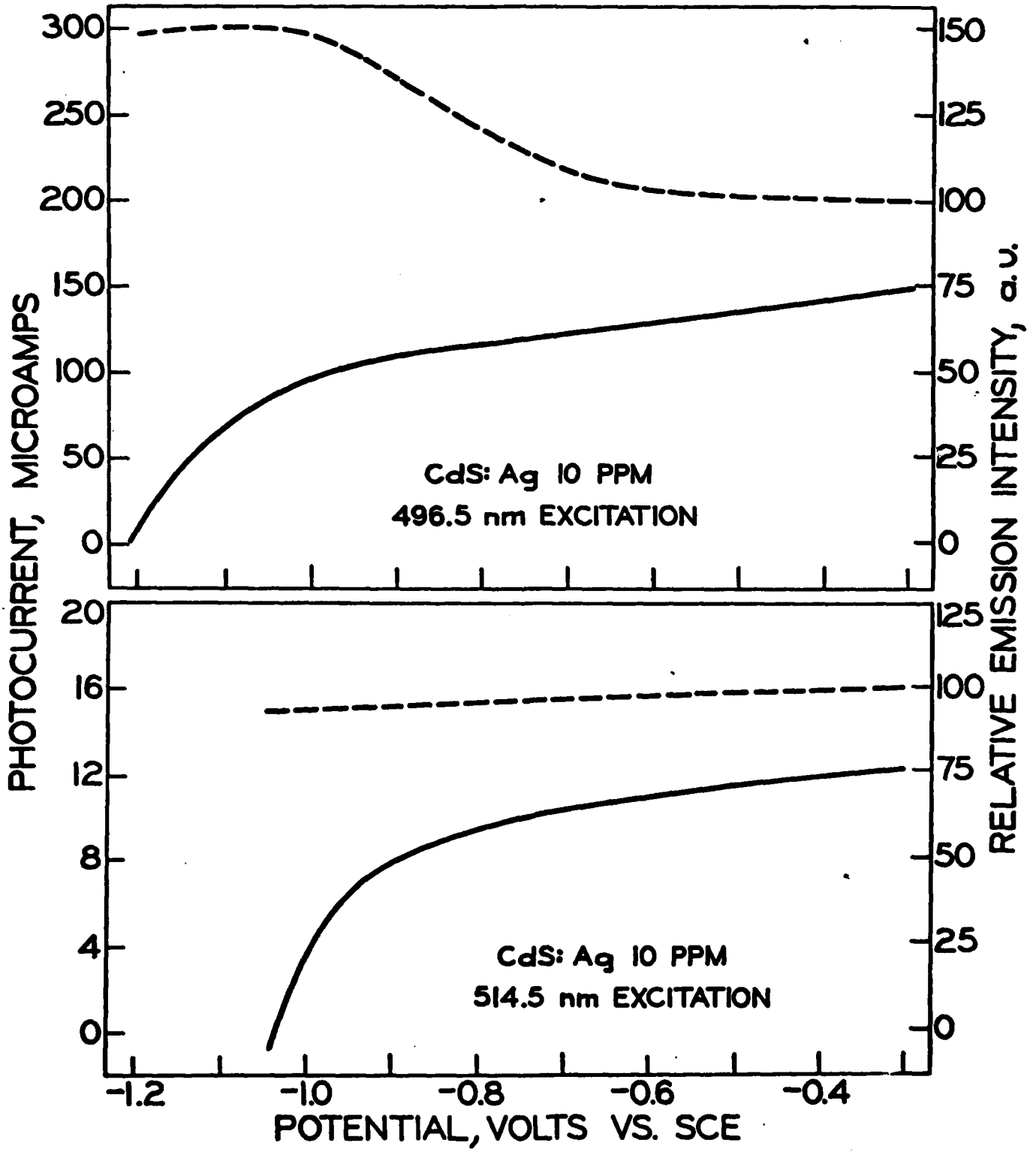
300
250
200
150
100
50
0
150
125
100
75
50
25
0
CdS: Ag 10 PPM
496.5 nm EXCITATION
20
16
12
8
4
0
125
100
75
50
25
0
CdS: Ag 10 PPM
514.5 nm EXCITATION
-1.2
-1.0
-0.8
-0.6
-0.4
POTENTIAL, VOLTS VS. SCE
PHOTOCURRENT, MICROAMPS
RELATIVE EMISSION INTENSITY, a.u.

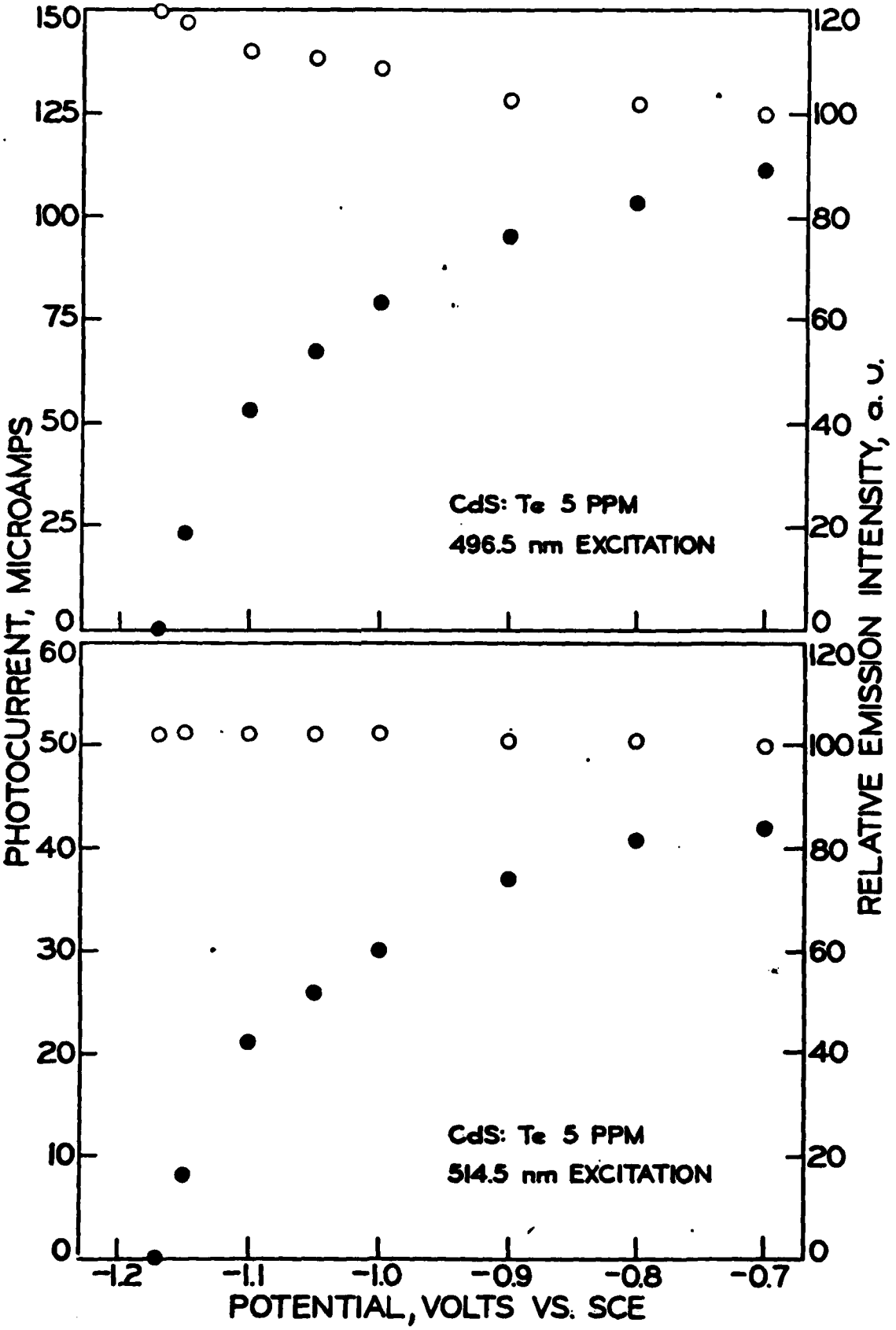
150
125
100
75
50
25
0
120
100
80
60
40
20
0
CdS: Te 5 PPM
496.5 nm EXCITATION
60
50
40
30
20
10
0
120
100
80
60
40
20
0
CdS: Te 5 PPM
514.5 nm EXCITATION
-1.2
-1.1
-1.0
-0.9
-0.8
-0.7
POTENTIAL, VOLTS VS. SCE
PHOTOCURRENT, MICROAMPS
RELATIVE EMISSION INTENSITY, a. u.

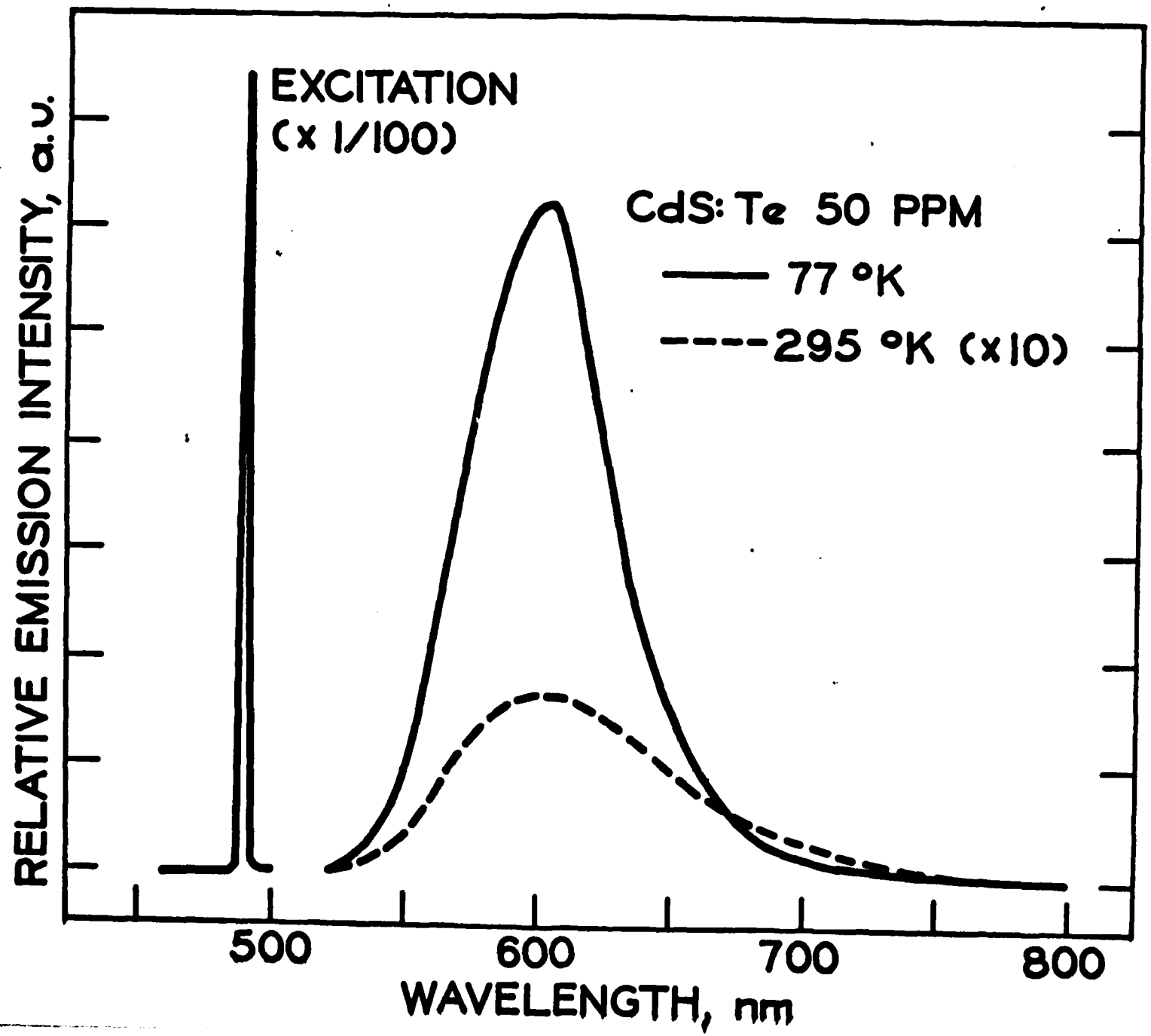
EXCITATION
(x 1/100)
CdS: Te 50 PPM
77 °K
295 °K (x10)
RELATIVE EMISSION INTENSITY, a.u.
500
600
700
800
WAVELENGTH, nm

TECHNICAL REPORT DISTRIBUTION LIST, GEN

	No. Copies
Office of Naval Research Attn: Code 472 800 North Quincy Street Arlington, Virginia 22217	2
ONR Branch Office Attn: Dr. George Sandoz 536 S. Clark Street Chicago, Illinois 60605	1
ONR Area Office Attn: Scientific Dept. 715 Broadway New York, New York 10003	1
ONR Western Regional Office 1030 East Green Street Pasadena, California 91106	1
ONR Eastern/Central Regional Office Attn: Dr. L. H. Peebles Building 114, Section D 666 Summer Street Boston, Massachusetts 02210	1
Director, Naval Research Laboratory Attn: Code 6100 Washington, D.C. 20390	1
The Assistant Secretary of the Navy (RE&S) Department of the Navy Room 4E736, Pentagon Washington, D.C. 20350	1
Commander, Naval Air Systems Command Attn: Code 310C (H. Rosenwasser) Department of the Navy Washington, D.C. 20360	1
Defense Technical Information Center Building 5, Cameron Station Alexandria, Virginia 22314	12
Dr. Fred Saalfeld Chemistry Division, Code 6100 Naval Research Laboratory Washington, D.C. 20375	1
U.S. Army Research Office Attn: CRD-AA-IP P.O. Box 1211 Research Triangle Park, N.C. 27709	1
Naval Ocean Systems Center Attn: Mr. Joe McCartney San Diego, California 92152	1
Naval Weapons Center Attn: Dr. A. B. Amster, Chemistry Division China Lake, California 93555	1
Naval Civil Engineering Laboratory Attn: Dr. R. W. Drisko Port Hueneme, California 93401	1
Department of Physics & Chemistry Naval Postgraduate School Monterey, California 93940	1
Dr. A. L. Slafkosky Scientific Advisor Commandant of the Marine Corps (Code RD-1) Washington, D.C. 20380	1
Office of Naval Research Attn: Dr. Richard S. Miller 800 N. Quincy Street Arlington, Virginia 22217	1
Naval Ship Research and Development Center Attn: Dr. G. Bosmajian, Applied Chemistry Division Annapolis, Maryland 21401	1
Naval Ocean Systems Center Attn: Dr. S. Yamamoto, Marine Sciences Division San Diego, California 91232	1
Mr. John Boyle Materials Branch Naval Ship Engineering Center Philadelphia, Pennsylvania 19112	1

TECHNICAL REPORT DISTRIBUTION LIST, GEN

	No. Copies
Dr. Rudolph J. Marcus Office of Naval Research Scientific Liaison Group American Embassy APO San Francisco 96503	1
Mr. James Kelley DTNSRDC Code 2803 Annapolis, Maryland 21402	1

TECHNICAL REPORT DISTRIBUTION LIST, 359

	No. Copies
Dr. Paul Delahay Department of Chemistry New York University New York, New York 10003	1
Dr. E. Yeager Department of Chemistry Case Western Reserve University Cleveland, Ohio 41106	1
Dr. D. N. Bennion Department of Chemical Engineering Brigham Young University Provo, Utah 84602	1
Dr. R. A. Marcus Department of Chemistry California Institute of Technology Pasadena, California 91125	1
Dr. J. J. Auborn Bell Laboratories Murray Hill, New Jersey 07974	1
Dr. Adam Heller Bell Laboratories Murray Hill, New Jersey 07974	1
Dr. T. Katan Lockheed Missiles & Space Co, Inc. P.O. Box 504 Sunnyvale, California 94088	1
Dr. Joseph Singer, Code 302-1 NASA-Lewis 21000 Brookpark Road Cleveland, Ohio 44135	1
Dr. B. Brummer EIC Incorporated 55 Chapel Street Newton, Massachusetts 02158	1
Library P. R. Mallory and Company, Inc. Northwest Industrial Park Burlington, Massachusetts 01803	1
Dr. P. J. Hendra Department of Chemistry University of Southhampton Southhampton SO9 5NH United Kingdom	1
Dr. Sam Perone Department of Chemistry Purdue University West Lafayette, Indiana 47907	1
Dr. Royce W. Murray Department of Chemistry University of North Carolina Chapel Hill, North Carolina 27514	1
Naval Ocean Systems Center Attn: Technical Library San Diego, California 92152	1
Dr. C. E. Mueller The Electrochemistry Branch Materials Division, Research & Technology Department Naval Surface Weapons Center White Oak Laboratory Silver Spring, Maryland 20910	1
Dr. G. Goodman Globe-Union Incorporated 5757 North Green Bay Avenue Milwaukee, Wisconsin 53201	1
Dr. J. Boechler Electrochimica Corporation Attention: Technical Library 2485 Charleston Road Mountain View, California 94040	1
Dr. P. P. Schmidt Department of Chemistry Oakland University Rochester, Michigan 48063	1
Dr. R. Richtol Chemistry Department Rensselaer Polytechnic Institute Troy, New York 12181	1

TECHNICAL REPORT DISTRIBUTION LIST, 359

	No. Copies
Dr. A. B. Ellis Chemistry Department University of Wisconsin Madison, Wisconsin 53706	1
Dr. M. Wrighton Chemistry Department Massachusetts Institute of Technology Cambridge, Massachusetts 02139	1
Larry E. Plew Naval Weapons Support Center Code 30736, Building 2906 Crane, Indiana 47522	1
S. Ruby DOE (STOR) 600 E Street Washington, D.C. 20545	1
Dr. Aaron Wold Brown University Department of Chemistry Providence, Rhode Island 02192	1
Dr. R. C. Chudacek McGraw-Edison Company Edison Battery Division Post Office Box 28 Bloomfield, New Jersey 07003	1
Dr. A. J. Bard University of Texas Department of Chemistry Austin, Texas 78712	1
Dr. M. M. Nicholson Electronics Research Center Rockwell International 3370 Miraloma Avenue Anaheim, California	1
Dr. Donald W. Ernst Naval Surface Weapons Center Code R-33 White Oak Laboratory Silver Spring, Maryland 20910	1
Dr. R. P. Van Duyne Department of Chemistry Northwestern University Evanston, Illinois 60201	1
Dr. B. Stanley Pons Department of Chemistry University of Alberta Edmonton, Alberta CANADA T6G 2G2	1
Dr. Michael J. Weaver Department of Chemistry Michigan State University East Lansing, Michigan 48824	1
Dr. R. David Rauh EIC Corporation 55 Chapel Street Newton, Massachusetts 02158	1
Dr. J. David Margerum Research Laboratories Division Hughes Aircraft Company 3011 Malibu Canyon Road Malibu, California 90265	1
Dr. Martin Fleischmann Department of Chemistry University of Southampton Southampton 509 5NH England	1
Dr. Janet Osteryoung Department of Chemistry State University of New York at Buffalo Buffalo, New York 14214	1
Dr. R. A. Osteryoung Department of Chemistry State University of New York at Buffalo Buffalo, New York 14214	1
Mr. James R. Moden Naval Underwater Systems Center Code 3632 Newport, Rhode Island 02840	1

TECHNICAL REPORT DISTRIBUTION LIST, 359

	No. Copies
Dr. R. Nowak Naval Research Laboratory Code 6130 Washington, D.C. 20375	1
Dr. John F. Houlihan Shenango Valley Campus Pennsylvania State University Sharon, Pennsylvania 16146	1
Dr. M. G. Sceats Department of Chemistry University of Rochester Rochester, New York 14627	1
Dr. D. F. Shriver Department of Chemistry Northwestern University Evanston, Illinois 60201	1
Dr. D. H. Whitmore Department of Materials Science Northwestern University Evanston, Illinois 60201	1
Dr. Alan Bewick Department of Chemistry The University Southampton, S09 5NH England	1
Dr. A. Himy NAVSEA-5433 NC #4 2541 Jefferson Davis Highway Arlington, Virginia 20362	1
Dr. John Kincaid Department of the Navy Stategic Systems Project Office Room 901 Washington, DC 20376	1
M. L. Robertson Manager, Electrochemical Power Sonices Division Naval Weapons Support Center Crane, Indiana 47522	1
Dr. Elton Cairns Energy & Environment Division Lawrence Berkeley Laboratory University of California Berkeley, California 94720	1
Dr. Bernard Spielvogel U.S. Army Research Office P.O. Box 12211 Research Triangle Park, NC 27709	1
Dr. Denton Elliott Air Force Office of Scientific Research Bldg. 104 Bolling AFB Washington, DC 20332	1

TECHNICAL REPORT DISTRIBUTION LIST, 051C

	No. Copies
Dr. M. B. Denton Department of Chemistry University of Arizona Tucson, Arizona 85721	1
Dr. R. A. Osteryoung Department of Chemistry State University of New York at Buffalo Buffalo, New York 14214	1
Dr. B. R. Kowalski Department of Chemistry University of Washington Seattle, Washington 98105	1
Dr. S. P. Perone Department of Chemistry Purdue University Lafayette, Indiana 47907	1
Dr. D. L. Venezky Naval Research Laboratory Code 6130 Washington, D.C. 20375	1
Dr. H. Freiser Department of Chemistry University of Arizona Tuscon, Arizona 85721	
Dr. Fred Saalfeld Naval Research Laboratory Code 6110 Washington, D.C. 20375	1
Dr. H. Chernoff Department of Mathematics Massachusetts Institute of Technology Cambridge, Massachusetts 02139	1
Dr. K. Wilson Department of Chemistry University of California, San Diego La Jolla, California	1
Dr. A. Zirino Naval Undersea Center San Diego, California 92132	1
Dr. John Duffin United States Naval Postgraduate School Monterey, California 93940	1
Dr. G. M. Hieftje Department of Chemistry Indiana University Bloomington, Indiana 47401	1
Dr. Victor L. Rehn Naval Weapons Center Code 3813 China Lake, California 93555	1
Dr. Christie G. Enke Michigan State University Department of Chemistry East Lansing, Michigan 48824	1
Dr. Kent Eisentraut, MBT Air Force Materials Laboratory Wright-Patterson AFB, Ohio 45433	1
Walter G. Cox, Code 3632 Naval Underwater Systems Center Building 148 Newport, Rhode Island 02840	1
Professor Isiah M. Warner Texas A&M University Department of Chemistry College Station, Texas 77840	1
Professor George H. Morrison Cornell University Department of Chemisty Ithaca, New York 14853	1